FOSSIL ENERGY

DOE/BC/14476-10
(DE92001060)

CHARACTERIZATION OF RESERVOIR ROCKS AND FLUIDS BY SURFACE ELECTROMAGNETIC TRANSIENT METHODS

Annual Report for 1990-1991

By
Pieter Hoekstra
Charles H. Stoyer
Bryan A. James
Mark W. Blohm

September 1992

Performed Under Contract No. AC22-90BC14476

Blackhawk Geosciences Inc.
Golden, Colorado

National Energy Technology Laboratory
National Petroleum Technology Office
U.S. DEPARTMENT OF ENERGY
Tulsa, Oklahoma

DISCLAIMER

This report was prepared as an account of work sponsored by an agency of the United States Government. Neither the United States Government nor any agency thereof, nor any of their employees, makes any warranty, expressed or implied, or assumes any legal liability or responsibility for the accuracy, completeness, or usefulness of any information, apparatus, product, or process disclosed, or represents that its use would not infringe privately owned rights. Reference herein to any specific commercial product, process, or service by trade name, trademark, manufacturer, or otherwise does not necessarily constitute or imply its endorsement, recommendation, or favoring by the United States Government or any agency thereof. The views and opinions of authors expressed herein do not necessarily state or reflect those of the United States Government.

This report has been reproduced directly from the best available copy.

DOE/BC/14476-10
Distribution Category UC-122

Characterization of Reservoir Rocks and Fluids by Surface Electromagnetic Transient Methods

Annual Report
1990-1991

By
Pieter Hoekstra
Charles H. Stoyer
Bryan A. James
Mark W. Blohm

September 1992

Work Performed Under Contract No. DE-AC22-90BC14476

Prepared for
U.S. Department of Energy
Assistant Secretary for Fossil Energy

Robert E. Lemmon, Project Manager
Bartlesville Project Office
P. O. Box 1398
Bartlesville, OK 74005

Prepared by
Blackhawk Geosciences, Inc.
17301 West Colfax Avenue, Suite 170
Golden, CO 80401

Table of Contents

List of Figures

ABSTRACT

The objectives of this research were to improve the interpretations of transient electromagnetic (TEM) measurements over two-dimensional subsurface structures. TEM is a surface electromagnetic method employed in fossil energy reservoir exploration and characterization. Electrical measurements find application in (i) assisting in fossil energy exploration mainly in areas where seismic methods yield inadequate data quality, such as volcanic covered terrain, permafrost areas, and the Rocky Mountain Overthrust; (ii) mapping contacts between hydrocarbon and brines in shallow producing horizons, and (iii) in monitoring enhanced oil recovery processes which cause zones of lower resistivity.

The work under this contract consisted of three tasks:

1) *Selection of a test site and acquisition of a high density, 3-component data set over the test site.* Important criteria for selection was the presence of a well defined two-dimensional (2-D) structures manifested in good electrical resistivity contrast, and relevance to fossil energy. The site selected was over a structure in the Basin and Range province of Nevada, with a geologic structure similar to the Trap Springs and Grant Canyon oil fields. Over this site, TEM data was acquired with conventional TEM equipment, but at a high station density with receiver locations illuminated by several transmitters. At each receiver station three components of the magnetic field were measured.

   The data were analyzed by conventional 1-D inversion and 1-D imaging procedures, so that the range of applications and limitations of 1-D analysis can be understood, and the degree of improvement resulting from 2-D imaging analysis could be evaluated. The results of 1-D analysis shows that 1-D analysis employing non-grounded loop transmitters agrees reasonably with known geology in terms of locations of faults, but often results in phantom resistivity stratification not expected from known geology. The survey layout employing grounded line transmitters was designed to maximize the influence of 2-D structures, so that data could not be effectively interpreted with 1-D methods. Survey design would have been completely different if 1-D interpretation were desired.

2) *Development of finite element modeling algorithms for computing 3-D EM fields over 2-D subsurface structures.* The finite element method is used to model the transient electromagnetic response of a two-dimensional earth structure to an

ungrounded square current loop source. E_x and H_x (where x is the strike direction) were used as potentials and other field components (E_y, E_z, H_y and H_z) are calculated from E_x and H_x using a second minimization method. The method was chosen over integral equation methods because of its versatility with respect to the kinds of 2-D models which it can handle.

The Lagrange density is written in terms of E_x and H_x for each frequency and integrated numerically over a rectangular mesh in which each rectangle is divided into four triangles. This is minimized to yield a set of simultaneous equations for the unknowns at each node in the rectangular mesh. The solution is carried out in the wavenumber (k_x) domain and inverse Fourier transformed to yield space domain solutions. The Fourier transform is again used to generate time domain fields from the frequency domain results.

Calculations were carried out on a Microway Number Smasher 860 with 8 Mbytes of memory, running the Intel i860 RISC processor. Each model run, consisting of 169 by 36 nodes, 24 spatial wavenumbers and 42 frequencies, required approximately 12 hours of time at a power of about 9 MFLOPS. Matrix size was 12,168 by 12,168 complex single precision numbers.

Comparison of currents calculated in the earth from E_x with analytical results for a homogeneous earth show that the method is working correctly. Ex calculations were then utilized in the 2-D imaging interpretation of the field data for two 2-D models: a two quarter-space model and a model which fairly well represents the final solution to the earth structure at the project site. The imaging of these data would not have been possible without the 2-D finite element code.

Calculation of other components (E_y, E_z, H_y and H_z) did not produce good results because the method used assumed a source-free region which is never the case when both source and measurements are made on the surface of a flat earth. Further research needs to be carried out to complete the development of the calculation of these fields and to thoroughly test the method.

3) *Development of TEM 2-D subsurface imaging method.* This method first interprets the patterns of current flow in the earth and then constructs an image resistivity section from

the interpreted current distributions. The 2-D imaging method differs from 1-D imaging in that a complete representation of the current distribution is utilized rather than a simple equivalent current filament. This requires use of a starting model. The current distribution in the earth is computed, as a function of time, for this initial model for all transmitter positions. Magnetic field profiles may be calculated from these current distributions using Biot-Savart's Law for purposes of comparing to the measured fields. All time slices of current distribution are perturbed by successive iterations to match the computed magnetic fields with the measured fields. The process is flexible in the type of subsurface structures it can accommodate, and matching of computed and measured magnetic fields can be simultaneously performed on both horizontal and vertical components of the field.

An image resistivity section is then constructed by position dependent weighted summation of the interpreted current within each pixel during position dependent time windows. This summation is ratioed to the summed current for the initial model to yield an image resistivity. A linear relationship between current and conductivity is assumed. The grid of image resistivity values are then contoured to yield the image resistivity section. The quality of the image resistivity section is a function of the starting model. If necessary, the entire imaging process may be repeated successively with each iteration using an improved starting model.

The 2-D imaging algorithms were tested on a synthetic data set produced from forwarded modeling, and subsequently it was employed in producing a geoelectric section of the test data set acquired over Basin and Range structure. The geoelectric section produced from 2-D imaging process compares well with known geology, and is an improvement on the geoelectric section derived from 1-D inversions and 1-D imaging. The improvements of the 2-D image are particularly evident in the absolute values of resistivities which correspond well with those expected from known geology.

EXECUTIVE SUMMARY

This report discusses the results of research to improve the interpretation of time domain electromagnetic (TEM) measurements in settings where subsurface conditions change rapidly both laterally and vertically. TEM is a surface geophysical method for determining the geoelectric section (lateral and vertical electrical resistivity variation) of the earth. The geoelectric section is then used in fossil energy reservoir exploration and development to infer geologic structure, brine versus hydrocarbon saturation in producing horizons, and for monitoring enhanced recovery processes. The research was conducted along three linked paths:

(1) *The selection of a test site and the acquisition of a high density TEM data set*. In present practices of TEM surveying data are acquired at low station density (usually 1 station per 1 to 10 km^2), and without complete characterization of the electromagnetic field. It was a fundamental concept of this research that improvement in lateral and vertical resolution of TEM interpretation demands (i) high station density, and (ii) measurements of 3-components of the magnetic field. Since such a data set did not exist, and since limitations exist in generating synthetic data sets, a data set was acquired over a well characterized site in the Basin and Range Province of Nevada. In this geologic Province there are several producing oil fields, and potential for additional discoveries exist. It is also an area where seismic reflection prospecting has often resulted in poor data quality.

This data set, in addition to its use in the research conducted under this contract, has also been supplied to researchers at the University of Utah and Lawrence Berkeley Laboratory. It is expected that this data set will be of great utility in testing computer processing and modeling algorithms in future years. The data is of high spatial density, complete in its characterization of the electromagnetic field, and was acquired over a well defined geologic structure which manifested itself in good electrical resistivity contrasts.

(2) *Finite element forward modeling*. Forward modeling of geoelectric sections, which characterize geologic structures, is an important tool in effective use of the TEM method. The utility of forward modeling is in (i) validating interpretations arrived at by either inversion or imaging processing, (ii) generating synthetic data sets for testing processing algorithms, and (iii) for planning effective field surveys. The path of research chosen for forward modeling of three-dimensional (3-D) transient electromagnetic fields over a 2-D

earth model was that of frequency domain finite element modeling with Fourier transformation to the time domain. The finite element method was chosen instead of integral equation methods because of the need for complete flexibility in generating 2-D models to simulate structural targets. The development, implementation, and verification of the finite element scheme turned out to be considerably more difficult than originally expected. Acquisition of a Microway Number Smasher 860 processor board was required to bring the project to the present state. Although further development is required to model measured fields on the earth's surface for a finite loop source, the finite element modeling algorithms were most valuable as a support tool for the 2-D imaging.

Verification of accuracy consisted of comparison with analytical results for currents inside a homogeneous earth. Moreover, the forward modeling was used to compute the currents in the earth for the geoelectric section of the test site in Nevada, and yielded correct results for the complex structure present.

(3) *TEM 2-D subsurface imaging*. The forward modeling of 3-D transient electromagnetic fields over 2-D earth by an integral equation method, such as those developed by other researchers previously, or by the finite element method developed in this research, remains a formidable task. The computer resources required for forward modeling will preclude for some time its effective use in inversion routines. It is partly for that reason that another approach of transient electromagnetic data interpretation in the presence of 2-D structure was developed and tested.

The TEM subsurface 2-D imaging method developed under this program derives the geoelectric section following the intermediate step of imaging the electrical current distribution in the ground. It utilizes a complete representation of distributed current flow on a subsurface grid, so that it can accommodate complicated geologic structures.

The major achievements of the imaging method under this research program are:

(i) The method has been proven to be fundamentally sound. It yields a geoelectric section consistent with known geology and with realistic absolute values of resistivity; and

(ii) The geoelectric section derived is based on matching both horizontal and vertical magnetic fields, and makes full use of high station density. This is an improvement on 1-D analyses where at present only the vertical magnetic field is utilized.

The improvements required to effectively employ 2-D imaging in routine practice appears now to be more technical than fundamental. For example, the iterative process of perturbing current distribution needs to be further automated, and the influence of the starting model on final results needs to be better understood. One especially attractive feature of the imaging approach is that it yields a thorough physical understanding of current flow in the ground. This in turn will result in better TEM survey design.

1.0 INTRODUCTION

The use of surface electrical geophysical methods in fossil energy exploration, reservoir characterization, and enhanced recovery monitoring is limited compared to the extensive use of seismic methods. There are, however, certain mapping objectives for which electromagnetic (EM) methodologies are well suited. Whenever mapping objectives can be delineated by their contrasts in electrical resistivity, electrical geophysical techniques can be considered, such as monitoring steam, combustion and water flooding, because these processes generally cause zones of low resistivity. Other objectives are mapping of brine versus gas saturation in shallow oil and gas reservoirs, and structural mapping in volcanic, overthrust, and permafrost terrain.

Two EM methods are in use for deep electrical measurements, - magnetotellurics (MT) and time domain EM (TEM) soundings. TEM is increasingly being applied in the depth range from 20 ft to about 10,000 ft. It offers the potential for lower sensitivity to ambient electrical and geologic noise, and better vertical and lateral resolution than MT.

This report presents the results of R&D efforts to develop procedures for interpreting high density TEM data to arrive at multi-dimensional geoelectric sections. The R&D proceeded along three linked paths:

1) *Selection of a test site and acquisition of a high density TEM data set.* Present practices of EM exploration consist of acquiring low density data and processing such data by 1-D analysis. Moreover, it is common to acquire and use only the voltages due to the vertical component of the magnetic field in deriving geoelectric sections, although equipment for measuring all three components is available.

   A test site was selected in the Basin and Range geologic province of Nevada over a 2-D structure with good geologic control, and with the structure strongly manifested in the geoelectric section. A high density 3-component TEM data set was acquired over this test site, and that data set was subsequently used in evaluating 2-D imaging algorithms, and for determining the range of applications and limitations of 1-D interpretations.

2) *Development of forward modeling algorithms for computing 3-D transient EM fields over 2-D structures*. Synthetic generation of EM fields has important uses in TEM interpretation technologies, such as

(i) Determining the range of applications of 1-D analysis. The acquisition of high density data sets may be too expensive for routine objectives for some time and 1-D analysis will remain an important tool. With a forward modeling capability the limitations of 1-D analysis over 2-D structures can be determined.

(ii) Testing of imaging algorithms over structures other than those acquired over the test site. The cost of field data acquisition limited collection of data to one test site. Subsequent testing of 2-D imaging algorithms can be performed on synthetic data sets. An important objective in the development of the forward modeling capability was to have it flexible in terms of structures it can accommodate.

3) *2-D Imaging of TEM data*. Traditional EM interpretation procedures have relied on computing the response for a certain geoelectric section and comparing that calculation to measured data. For 1-D interpretation, these processes are accommodated in ridge regression inversion programs. This approach breaks down when the geoelectric section significantly departs from horizontally stratified (1-D) layers. Moreover, the necessary computer resources required for modeling 2-D and 3-D structures precludes at present its incorporation in inversion programs. In the 2-D imaging procedure developed the geoelectric section is derived from imaging the current distribution in the earth. The subsurface is divided into pixels and in each pixel the current flow, as a function of time, is calculated for an initial geoelectric model. For each time slice, the magnetic field profile on the earth's surface is computed from the current distribution by Biot-Savart's Law. By iterative processes the current distributions are altered until a match is obtained between measured and computed magnetic fields.

This method of analysis differs in important aspects from the present practice of interpretation of TEM data, in that:

(i) The method is flexible in type of structures of the subsurface it accommodates, so that some of the limitations of 1-D interpretation are removed;

(ii) Two components of the magnetic field are matched in the interpretation.

The imaging method was tested in this R&D program on a synthetic data set derived from forward modeling, and was subsequently used on the test data to produce a geoelectric section.

This report provides a condensed review of all three aspects of the R&D effort. The site selection procedures, the geology of the selected test site in Nevada, and a description of the high density data set acquired are described in Section 2.0. Also, this section contains an evaluation of the range of applications and limitations of 1-D processing over this strong 2-D structure. The approach employed, the theory of, the verification of, and the hardware used for the forward modeling are described in Section 3.0. The physical concepts of the imaging process, the use of the imaging process in acquired test data, and the results produced are given in Section 4.0. Finally, conclusions of this R&D effort are given in Section 5.0.

In addition to this condensed final report, three Topical reports have been issued under this contract. These reports contain details about each aspect of the work: (i) Site selection and acquisition of a high density data set; (ii) development of forward modeling algorithms for computing 3-D transient EM fields over 2-D structures; and (iii) 2-D TEM imaging.

2.0 SITE SELECTION AND ACQUISITION OF HIGH DENSITY, 3-COMPONENT TEM DATA SET OVER TEST SITE

2.1 Purpose

Electromagnetic surveys for hydrocarbon reservoir exploration and development are presently characterized by a low station density. Furthermore, it is common to acquire only the electromotive force due to the time derivative of the vertical magnetic field (e.g., Hoekstra and Blohm, 1990; Bernstein et al, 1977). This low station density and incomplete characterization of the EM field preclude the use of past data sets in testing forward modeling and imaging algorithms for resolving 2-D or 3-D structures.

Alternatives to acquiring field data sets over known geologic structures are the generation of synthetic data sets from numerical computation and physical modeling. The generation of data sets by numerical computations is at present limited to relatively simple structures with relatively large resistivity contrasts. An excellent example of the utility of physical modeling is the work by Wilt (1991). From such scale modeling many practical, empirical conclusions can be drawn, such as the influence of transmitter-receiver arrays, and the general behavior of EM fields.

There are, however, limitations to generating realistic synthetic data sets, either from physical modeling or numerical computations, such as simulating geologic noise which, in TEM, varies with time and with the component of the EM field. Since high density 3-component data sets are not now available, the acquisition of a data set over a well defined structure was an important part of this research effort.

2.2 Site Selection and Site Geology

In the evaluation of new inversion and imaging algorithms on a field data set, it is important to have geologic structures well characterized by geologic mapping, drilling, and other surface geophysical interpretations. Furthermore, the geologic structure must be recognizable in a geoelectric section.

During the site selection process over 30 prospective sites were evaluated and site visits were made to 3 sites. The main selection criteria used were

- presence of structures that can be represented by a 2-D geometry, and are manifested in a geoelectric section with good resistivity contrasts,

- availability of ground truth from drilling, geologic mapping, and complimentary geophysical data,

- relevance of geologic setting to occurrence of hydrocarbons,

- ease of access and permitting.

Many prospective sites relevant to hydrocarbon reservoir enhanced oil recovery processes were eliminated due to a lack of measurable resistivity contrasts, or excessive infrastructure that would interfere with EM measurements. The site finally selected is located approximately 15 miles north of Carlin, Nevada in Eureka County. A site location map is shown in Figure 1. The study area is controlled by Newmont Exploration Limited and Euro-Nevada Mining Corporation, Inc.

The site is located in the Basin and Range geologic province. A geologic map of the immediate vicinity of the site is shown in Figure 2, and a geologic cross-section A-A' is shown in Figure 3. The geology of the study area consists of Devonian and Silurian age Jasperoid and Roberts Mountain Formation outcropping on the west, and Quaternary age alluvium on the east. The Roberts Mountain Formation is described as a silty laminated dolomitic limestone and the Quaternary alluvium is described as recent valley and stream channel fill. The Jasperoid and Roberts Mountain Formation are normal faulted with down-dropped blocks to the east and covered by the Quaternary alluvium. The main fault through the area is the Tuscarora Fault which is projected to strike approximately north-south through the study area.

The geologic cross-section of Figure 3 is to a large extent based on the lithologic logs of drill holes EUR49 and EUR53. Detailed gravity data in the area suggests that the faulting interpreted between the boreholes is secondary to the main Basin and Range fault which occurs to the east of borehole EUR53 and has an estimated offset in excess of 5,000 ft. Figure 4 is a contour map of depth to bedrock based on drill holes (EUR49, 50, 51, 53 and 54) and gravity modeling. Also shown on Figure 4 is the locations of the Tuscarora Fault from a geologic map. The depth to bedrock contour map shows that the orientation of the structure is north-south, approximately parallel to the contact with outcrop and the mapped Tuscarora fault. The projected location of the Tuscarora fault shows an approximate north-south strike for at least 1 mile on either side of boreholes EUR49 so that the structure in the vicinity of boreholes EUR49 and EUR53 can be adequately described as 2-D.

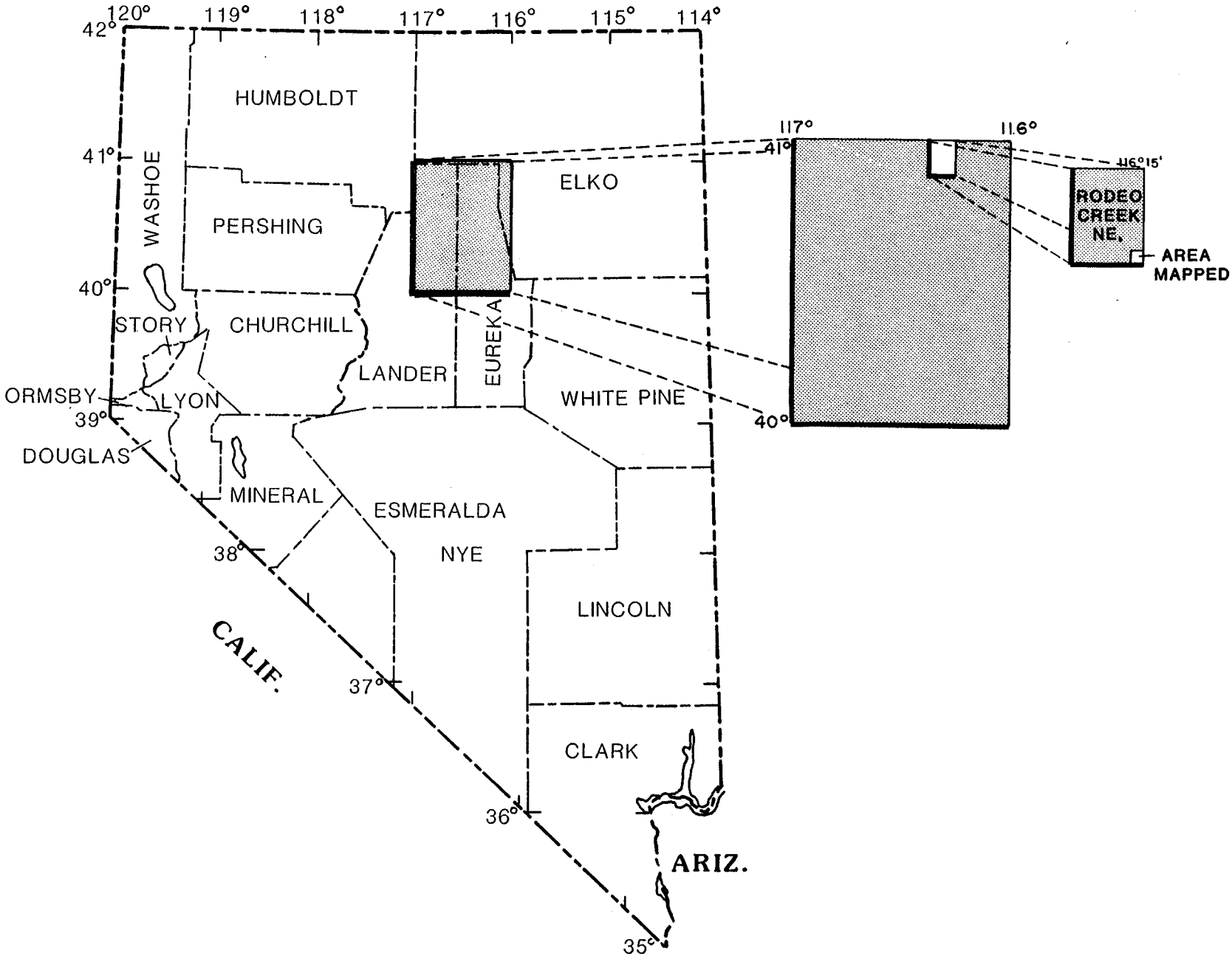

Figure 1 Location map of test site

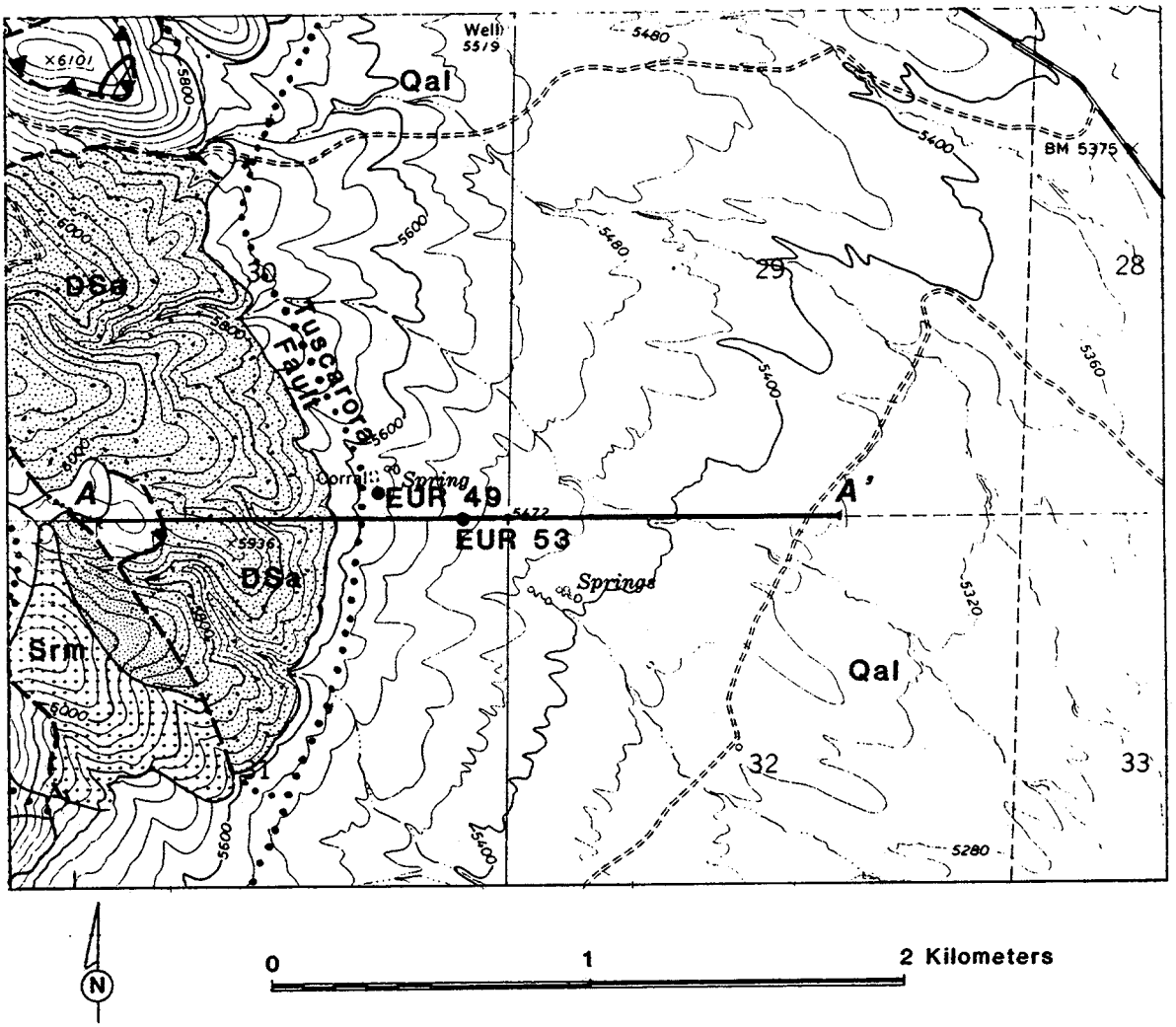

● Newmont Exploration Ltd. boreholes

Qal ALLUVIUM - Most recent valley and stream channel fill.

DSa JASPEROID - White, black, gray, maroon, violet, yellow, green, and brown laminated to massive jasperoid. Grades into Roberts Mountains Formation and overlaying unnamed limestone.

Srm ROBERTS MOUNTAINS FORMATION (Silurian) - Typically a silty laminated dolomitic limestione weathering into thin plates: generaly poorly exposed. In the 1,550-foot-thick section measured west of Sheep Creek Canyon, medium-grained bioclastic limestone beds up to a few feet thick are interbedded with the laminated limestone. Black siliceous shale beds and lenses less than 1 inch thick occur within the lower 100 feet and uppermost 275 feet of the laminated limestone.

Figure 2 Geologic map of test site

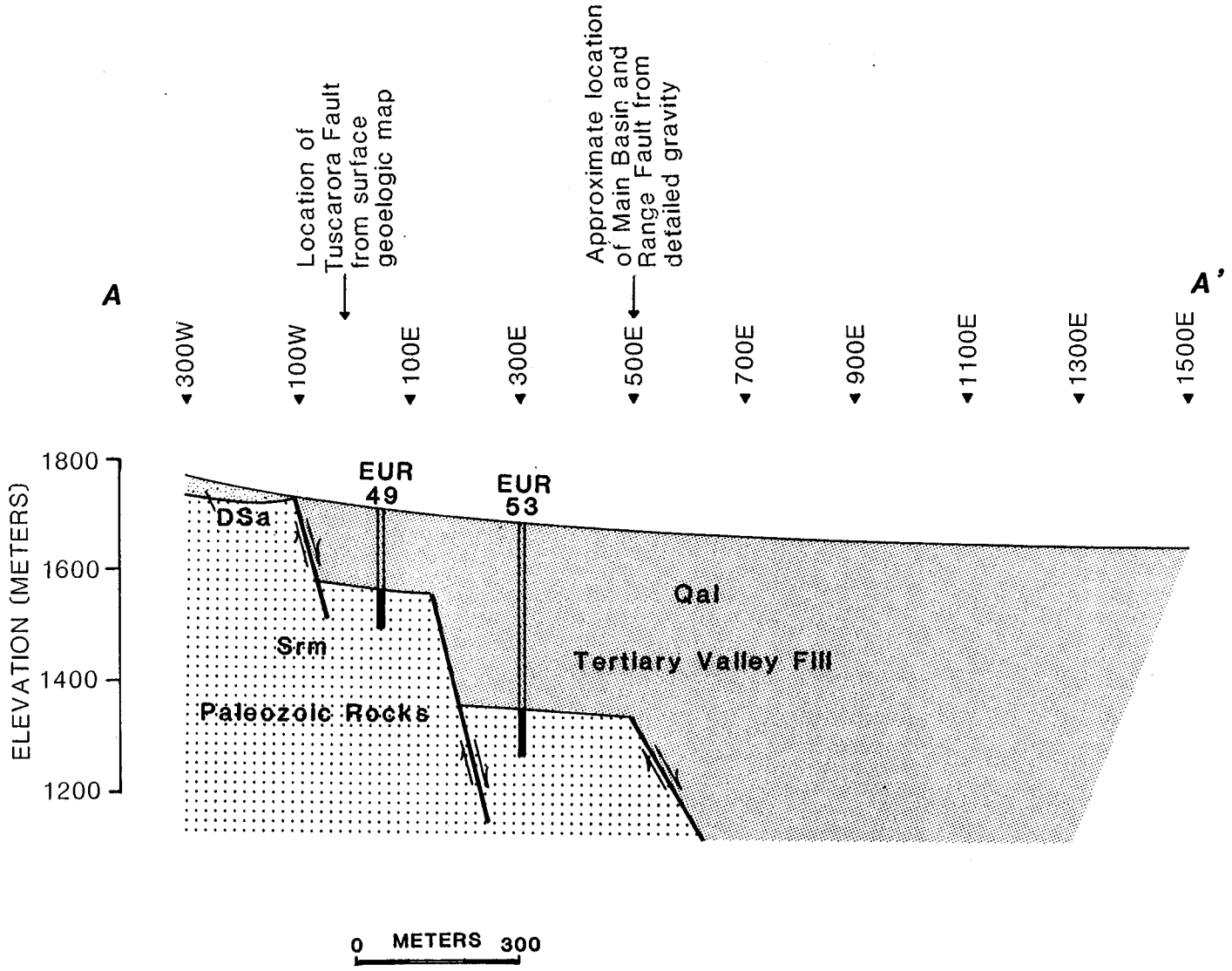

Figure 3 Geologic cross-section A-A' through test site

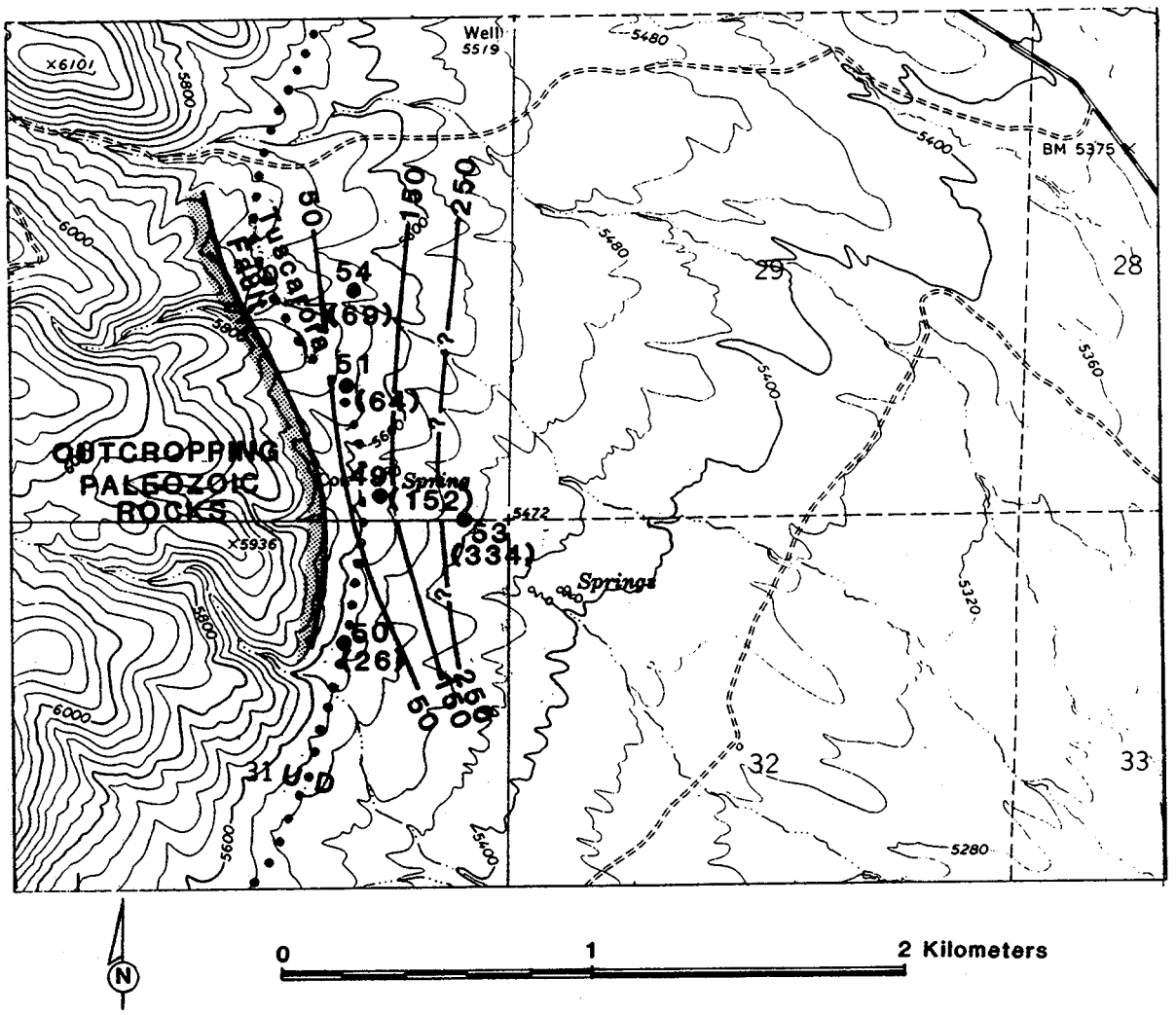

●50 Newmont Exploration Ltd. Boreholes

(26) Depth to bedrock in meters

Figure 4 Contour map of depth to bedrock from gravity modeling at test site

From oil and gas, precious metals, and geothermal exploration in the Basin and Range Province the range of geoelectric parameters for the different formations are also relatively well known. Figure 5 shows characteristic ranges of electrical resistivity based on Hoekstra et al (1989), and Figure 6 is a geoelectric model along A-A'. Thus, the fault is expected to be manifested by a major contrast in electrical resistivity.

Exploration and development of hydrocarbon resources in the Basin and Range has been hindered by the relatively low quality of seismic data. The occurrence of welded volcanics within the Tertiary Valley fill, high velocity Paleozoics in the Range, and high-angle faults are the major cause of the difficulties in acquiring high quality seismic data. Potential field methods and EM exploration have been major tools for delineating reservoirs. Figure 7 (Duey, 1979) shows the geologic setting in Railroad Valley, Nevada, i.e., Trap Springs Field and Grant Canyon Field. In the Railroad Valley, Basin and Range extension faulting, through either horst and graben or lystric-style movement dominates the geology of the survey area. Railroad Valley is an asymmetric Basin bounded by Grant Range to the east and Pancake Range to the west. There is a steep, west dipping, lystric-style fault with 2 to 4 km of vertical displacement comprising Railroad Valley's eastern flank. The western flank dips more gently to the east and is also bounded by lystric style faulting. The geologic setting of these two fields is similar of the site selected near Carlin, Nevada.

2.3 Acquisition of TEM Data

TEM is a controlled source EM method (Kaufman and Keller, 1983) and two common types of sources are employed, (i) grounded line sources with magnetic dipole receivers offset from the line, and (ii) non-grounded square transmitter loops with magnetic dipole receivers positioned in the center and at positions offset from the center. These two types of transmitter and receiver geometries are illustrated in Figure 8. The most common receivers employed are multi-turn air coils and the effective areas of the receivers employed varies from about 100 m^2 to 10^5 m^2 (Hoekstra and Blohm, 1990). The receivers with large effective area are often seismic cables laid out over the ground surface, but coils with effective area of 1000 m^2 and less are wound on a rigid mandrel. With these latter coils both vertical and horizontal components of the field can be measured.

A common system waveform of TEM systems is shown in Figure 9. The current driven through the transmitter loop is a half-duty cycle waveform and a steady current is terminated by a linear ramp. Ramp time depends on peak current and dimensions of transmitter loops, and is about several hundred microseconds for the exploration depth required in hydrocarbon exploration.

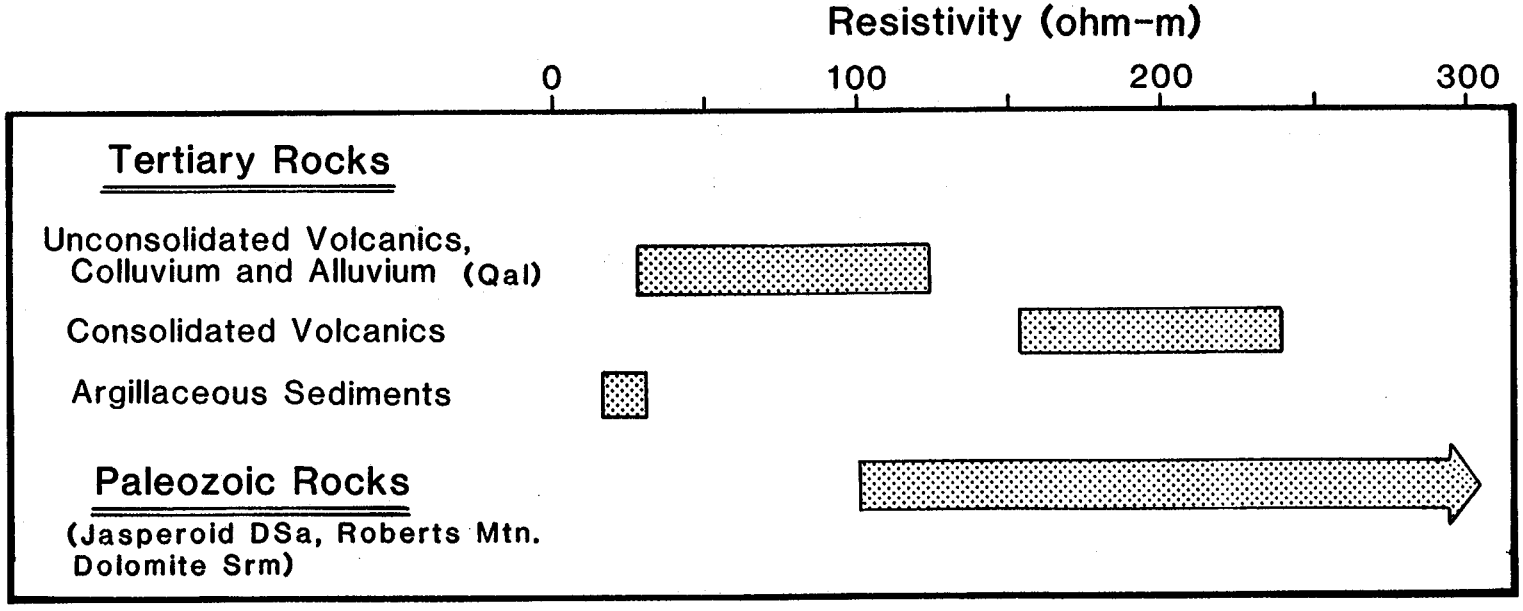

Figure 5 Characteristic ranges of electrical resistivity of formations near test site

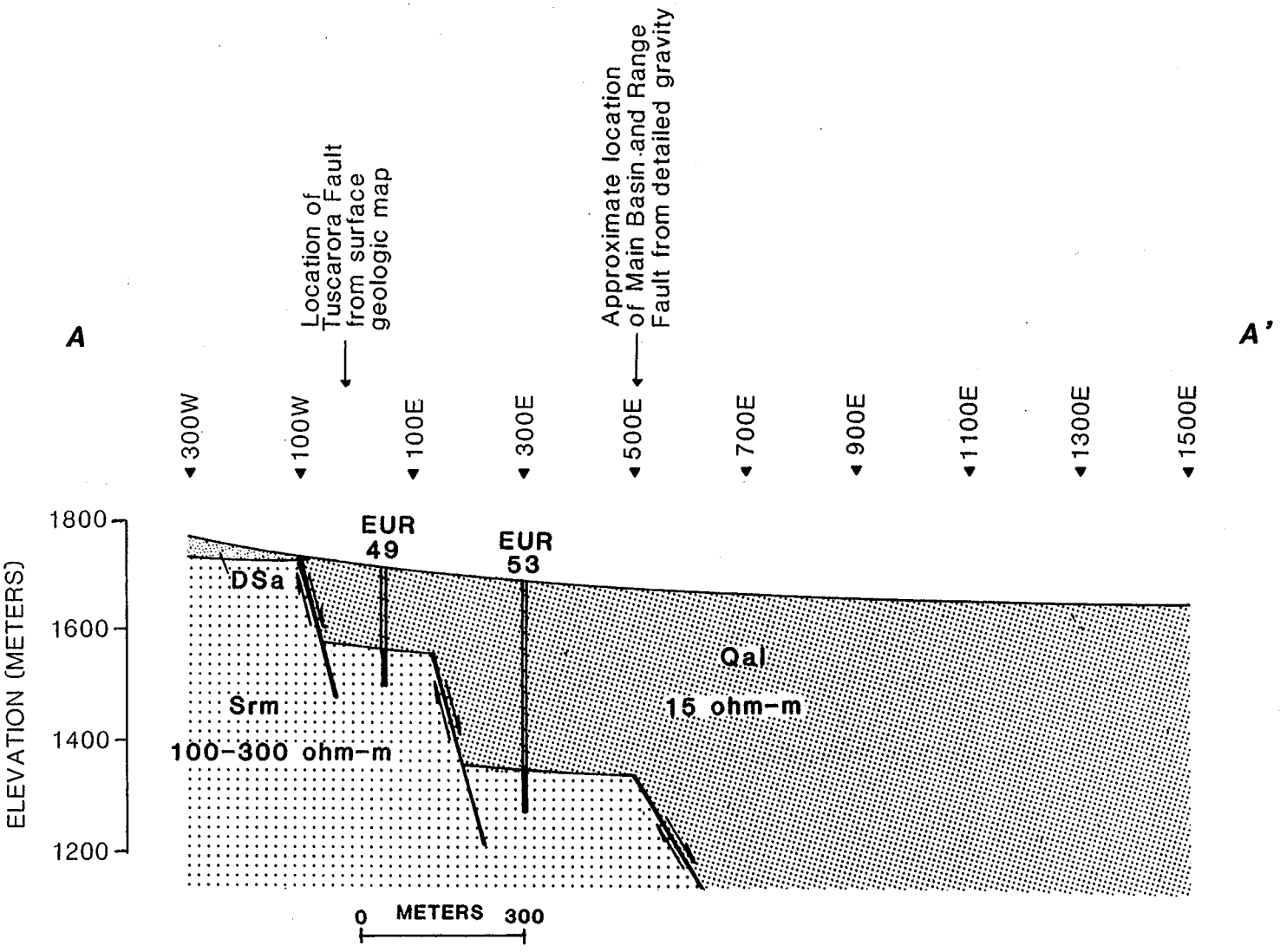

Figure 6 Geoelectric section for geologic cross-section A-A

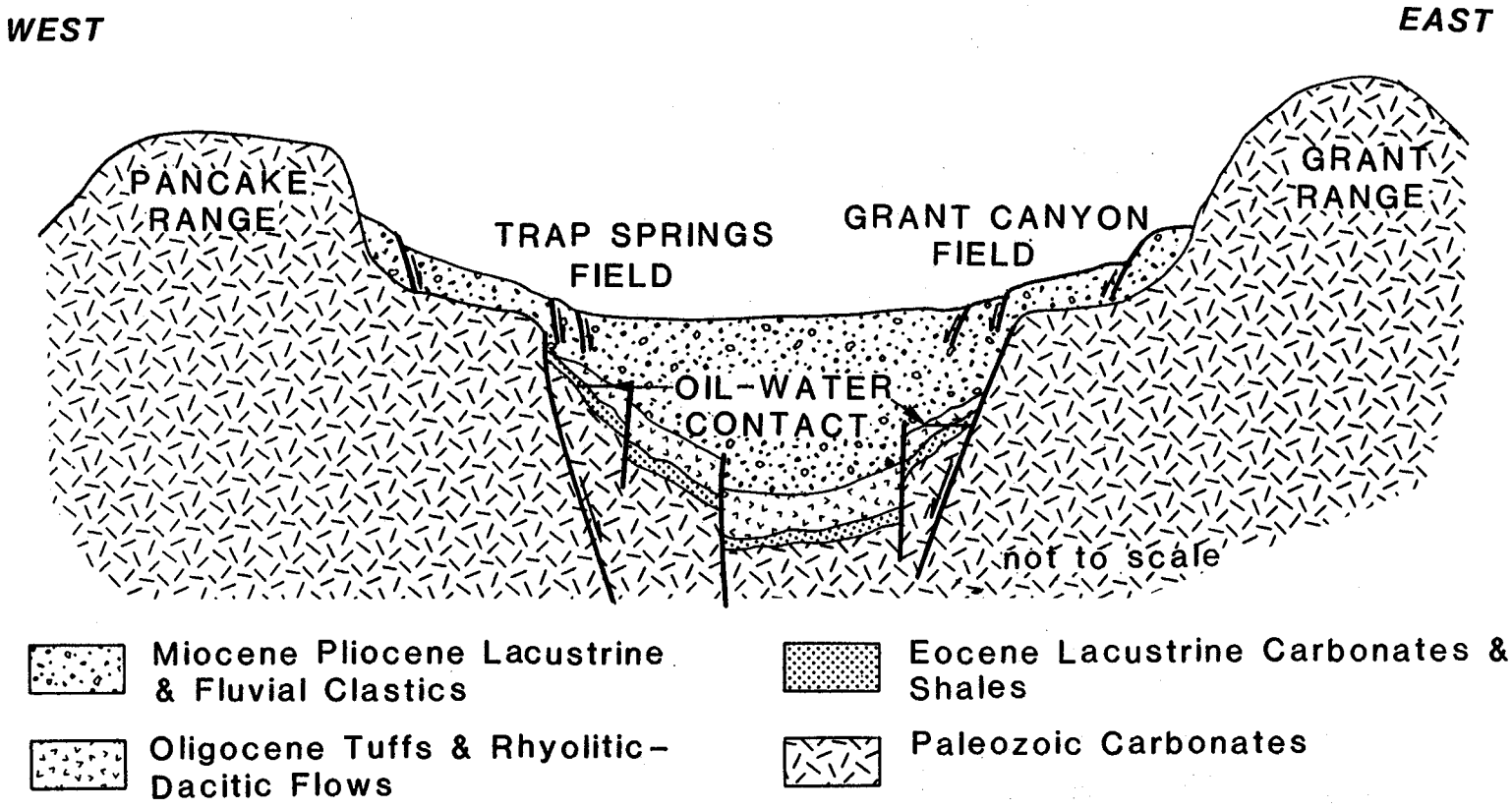

Figure 7 Geologic model typical of Trap Springs and Grant Canyon oil fields in Railroad Valley, NV

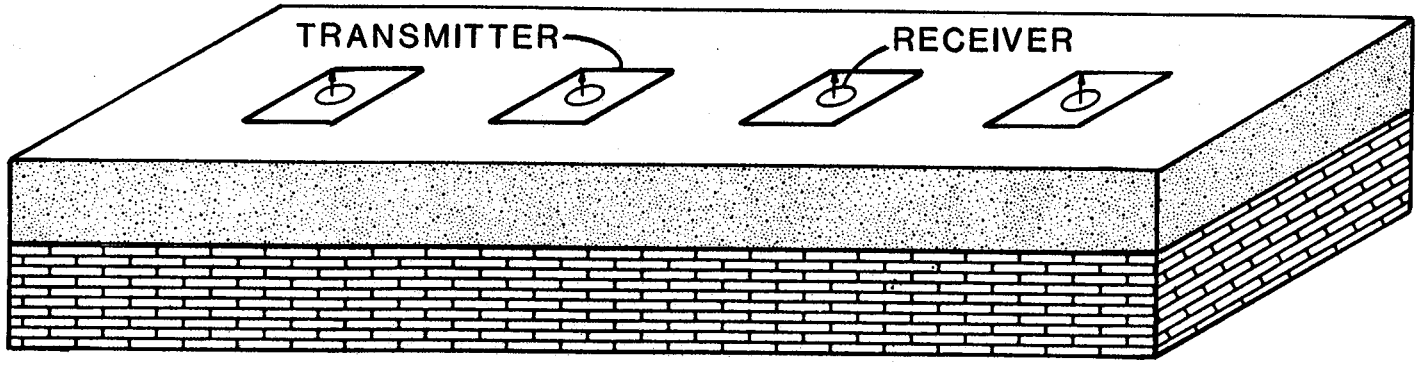

a) a loop-loop (central-loop) array, in which the transmitter is a non-grounded loop and a receiver is positioned in the center:

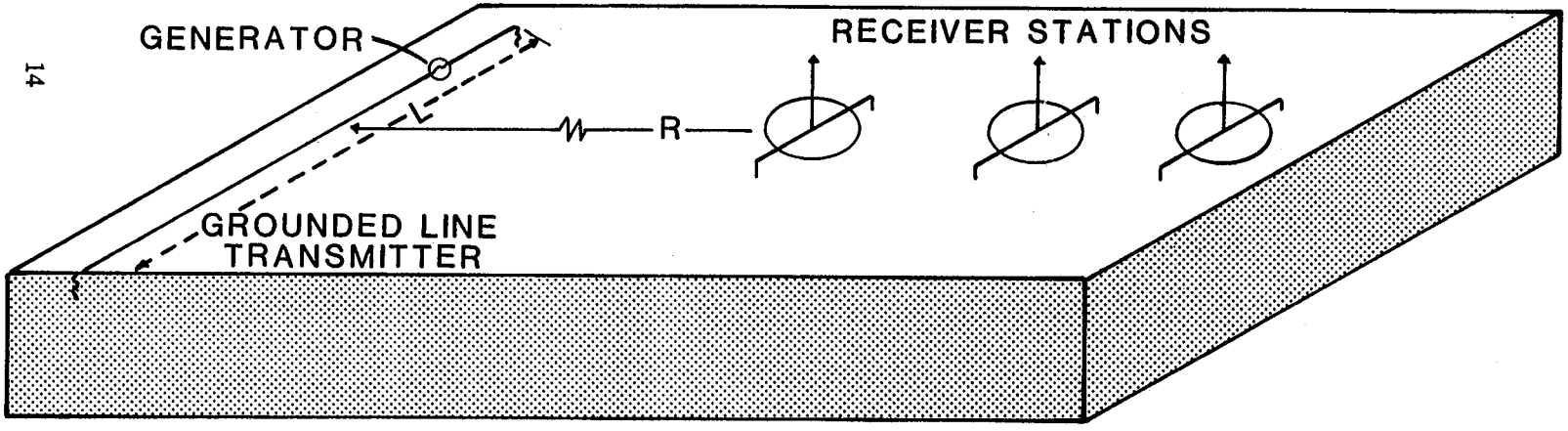

b) a grounded line array, in which the transmitter is a grounded line and the receiver is offset from the center.

Figure 8 Illustration of grounded line and non-grounded loop transmitters

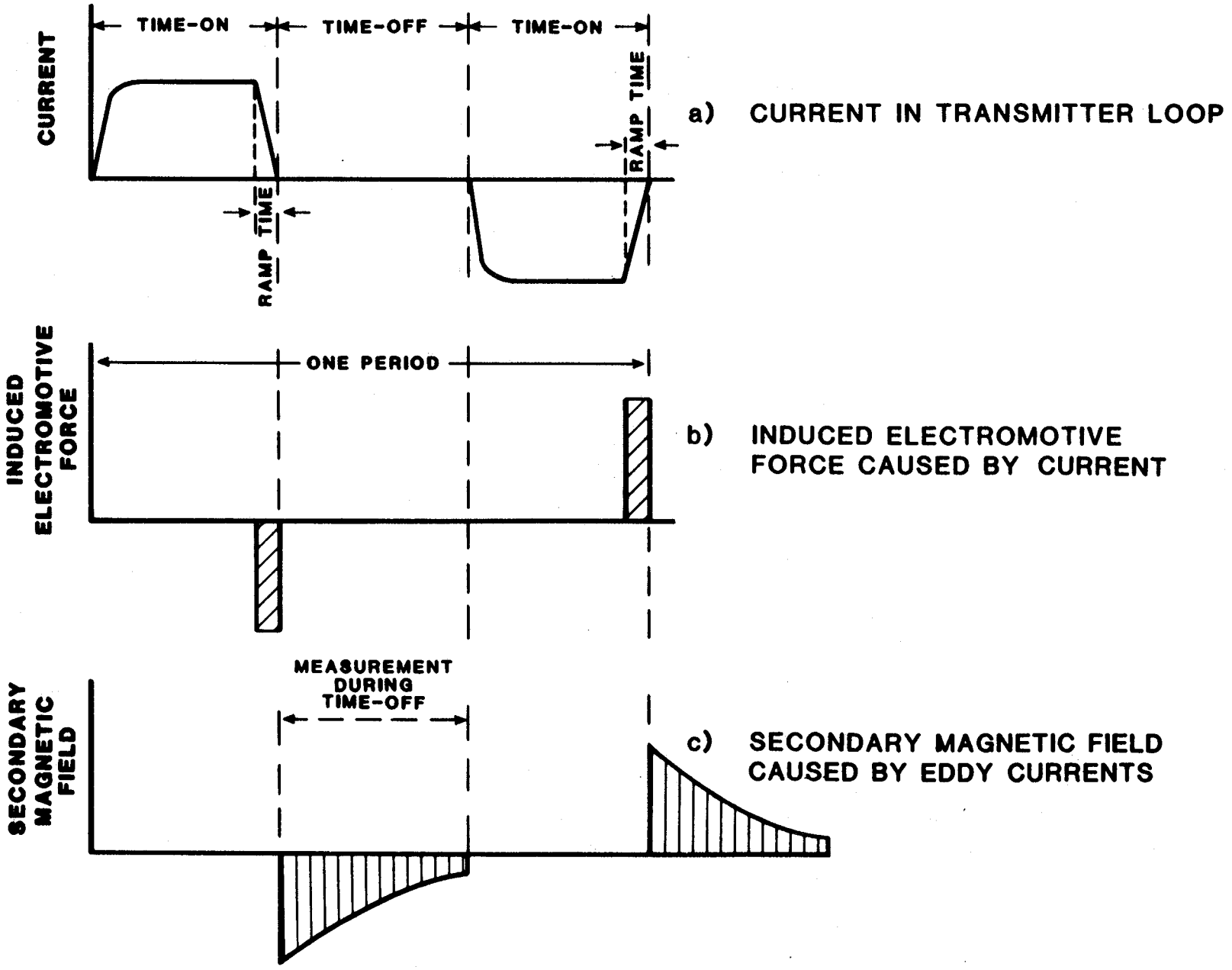

Figure 9 System waveforms of TEM system

Over the test site data was acquired both with grounded line and non-grounded loop transmitters. The layout of transmitters and receivers is shown in Figures 10a and 10b. The receiver positions were located along a line perpendicular to the Basin and Range fault. At each receiver station the EM field was recorded from several transmitter positions, and 3 components of the EM field were measured.

2.4 1-D Inversions of the Transient Emf's Measured in the Center of Non-Grounded Square Transmitter Loops

Present practice of TEM for hydrocarbon exploration consists of inversion and interpretation by 1-D algorithms. At each receiver station a 1-D geoelectric profile is derived, and typically a 2-D geoelectric cross-section is constructed from a series of 1-D profiles. To understand the limitations of 1-D interpretation, and to evaluate the improvement resulting from 2-D and 3-D forward modeling and imaging, the data acquired were processed by 1-D inversion and 1-D imaging algorithms. Subsequently, known geology from geologic mapping, drill holes, and complimentary geophysical data was superimposed on the derived geoelectric section.

The inversion algorithms used are those initially published by Inman (1975) using a forward solution taken from Anderson (1979). Figure 11 shows three apparent resistivity curves and the geoelectric profiles of the 1-D inversions. Figure 12 shows the geoelectric section created by linking the results of the 1-D inversions from the center-loop measurements. Superimposed on the geoelectric section is the geologic information.

From a comparison of the geoelectric section and the geologic information, the following conclusions can be derived:

(1) The position of the 2-D structure near station 150E based on drill holes and geologic mapping is inferred at approximately the same location from the geoelectric section. On the other hand, the position of the 2-D structure mapped beneath station 500E is not evident in the geoelectric section derived from 1-D inversions.

(2) For soundings west of the contact (west of 100W), the interpreted section differs from known geology. In this area (300W to 100W) a relatively conductive (42 to 23 ohm-m) layer is obtained from 1-D inversion, but there is no apparent physical reason for such relative low resistivities in the geologic section. The outcropping of Jasperoids west of station 100W are expected to be of high resistivities.

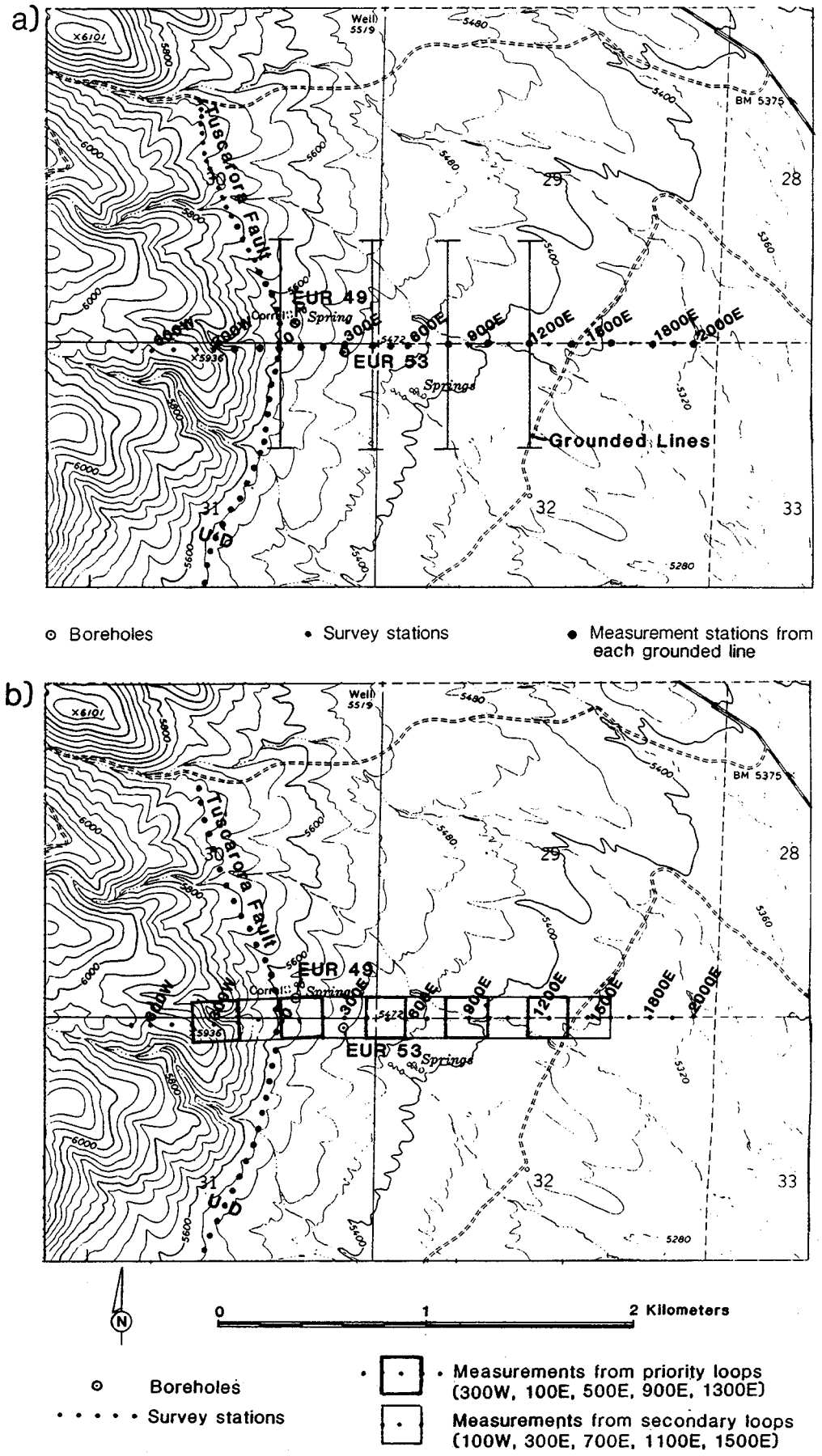

Figure 10 Layout of transmitter-receiver locations at test site; a) grounded line transmitters, and b) non-grounded loop transmitters

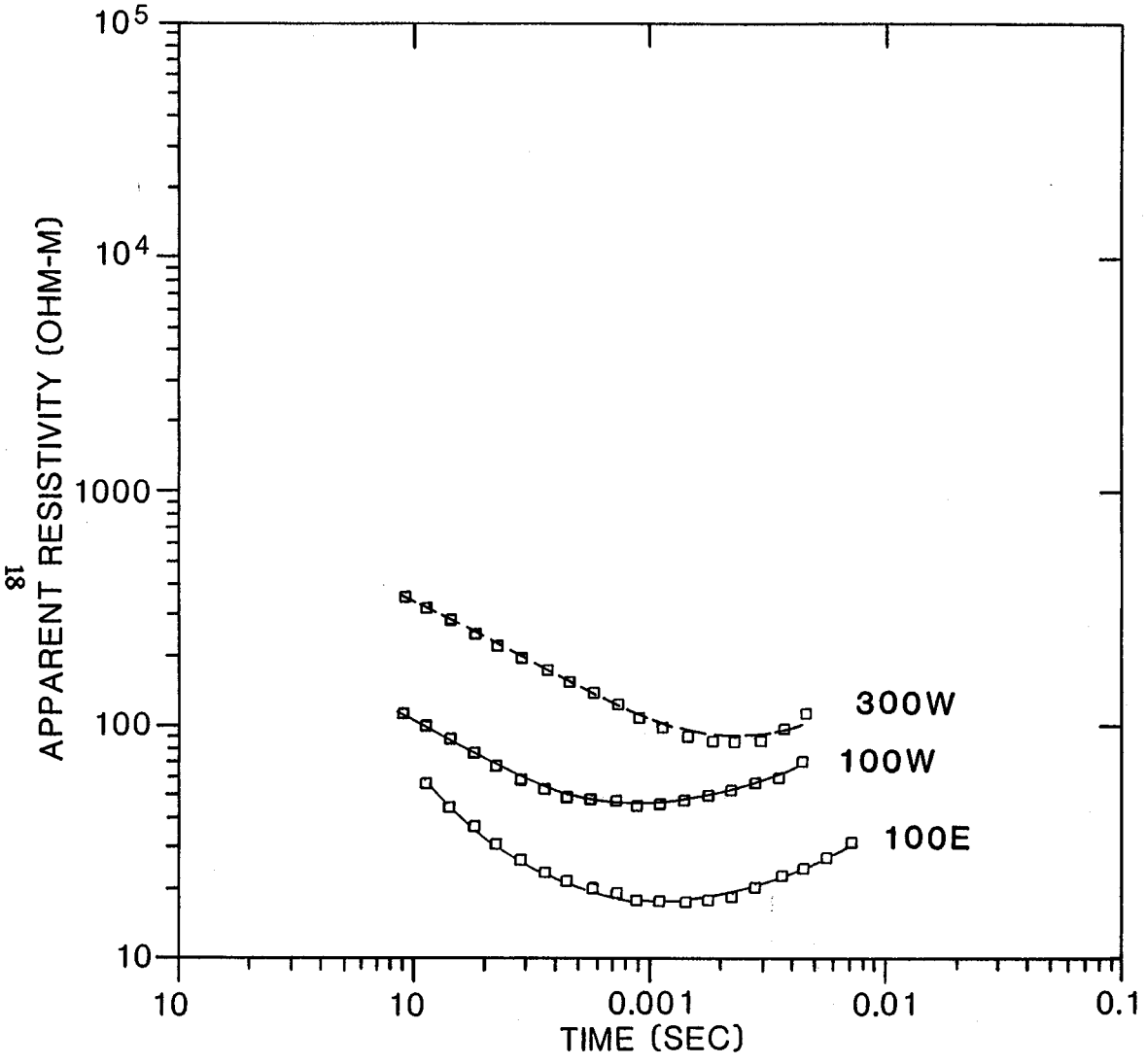

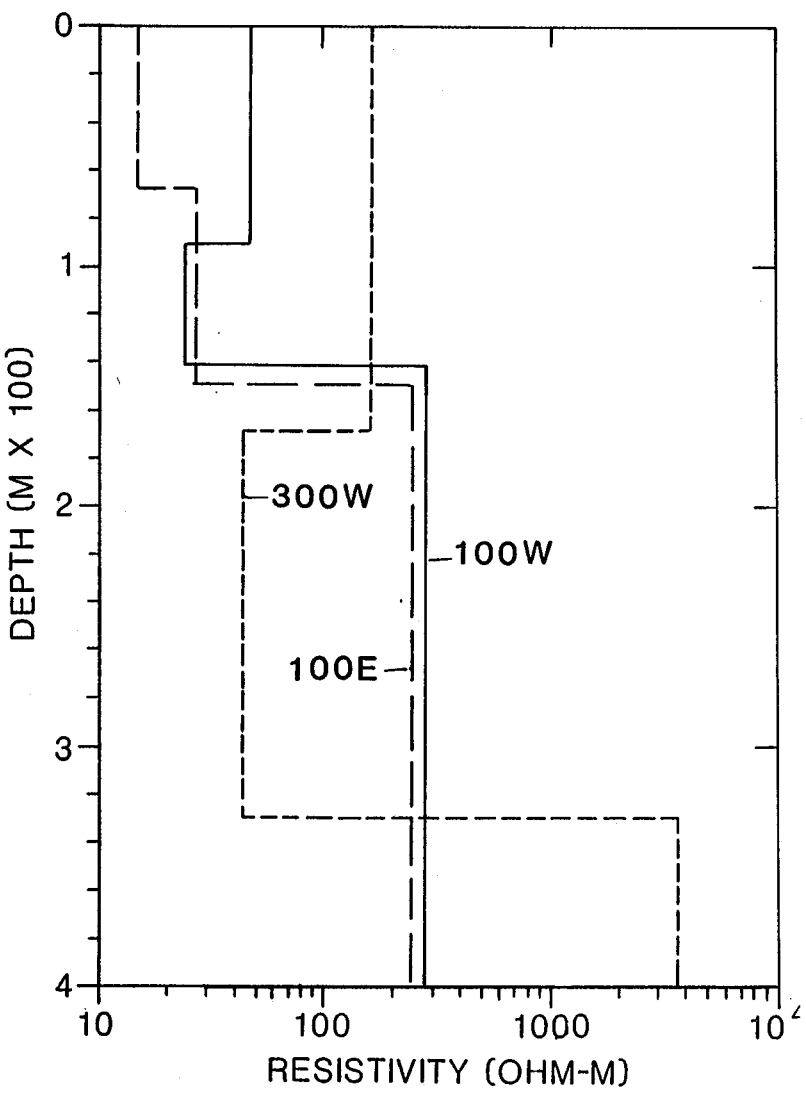

Figure 11 Three late stage apparent resistivity curves acquired at test site and their 1-D inversion

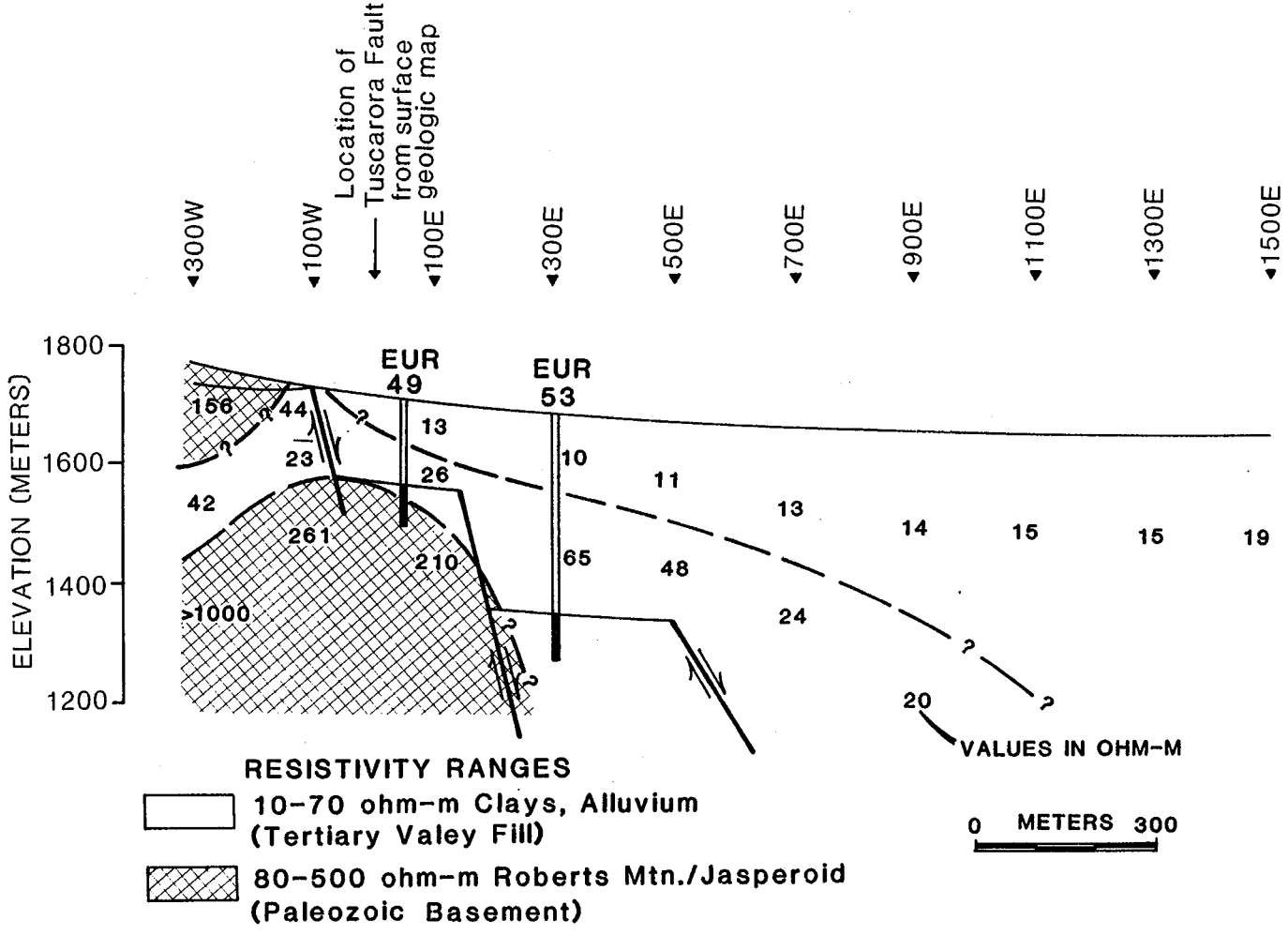

Figure 12 Geoelectric section derived from inversion of voltages due to vertical magnetic field in center of loop

Thus, 1-D inversions of TEM data over 2-D structures have their utility in that the presence and approximate location of the structure can be determined. These inversions have their limitations, in that geoelectric sections near 2-D structures are derived with absolute values of resistivities substantially deviating from values expected from known geology.

2.5 1-D Imaging of Transient Emf's Measured in the Center and Outside Non-Grounded Square Transmitter Loops

The imaging algorithms used are those described by Eaton and Hohmann (1989). In their method responses measured in the vicinity of each source are matched at each delay time by the magnetic field of a single current filament in free space. This filament, which moves downward with time, is an image of the surface loop. A continuous resistivity profile with depth is estimated from the velocity of migration of the current filament.

To obtain a cross-sectional image the data for each sounding were plotted in a vertical section and contoured as shown in Figure 13. Again, the geologic section derived from drill holes and geologic mapping is superimposed for comparison. From this comparison the following conclusions can be drawn:

(1) The highest resistivities obtained over the Range (west of station 0W) are about 90 ohm-m, and the resistivities gradually decrease eastward over the Basin. The absolute resistivity values over the Range are lower than expected from known geologic information. Comparing the known geologic data with the geoelectric section, the 20 ohm-m contour appears to best reflect the location and depth of the Basin and Range fault. In practice, selection of a resistivity contour to represent the interface between Tertiary valley fill and Paleozoic rock is subjective, and this subjectivity must be considered a main limitation of 1-D imaging.

(2) In these same areas the resistivity values derived from 1-D inversions are at least a factor of two larger. This discrepancy is expected to be due to limitations inherent in the 1-D imaging procedure over resistive ground. In more conductive areas (e.g., from 500E to 1500E) the resistivity values obtained with the 1-D inversions and 1-D imaging are in agreement.

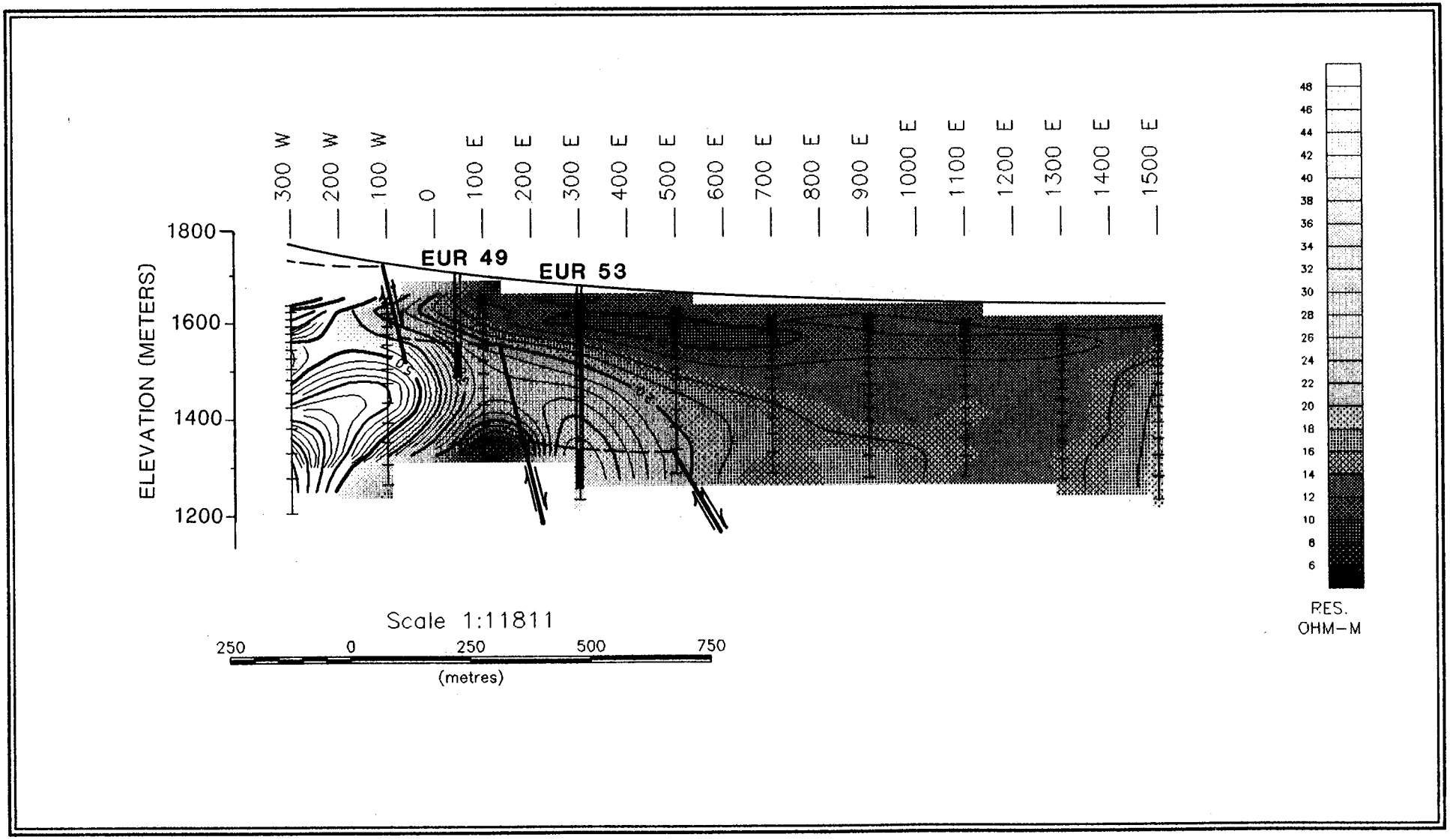

Figure 13 Geoelectric section derived from 1-D imaging of voltages due to vertical magnetic field from non-grounded loop transmitters. Geologic and drill hole information is superimposed on section

2.6 1-D Inversion of the Transient Emf's Measured from Grounded Line Transmitters

Grounded line transmitters at one time were common in deep TEM exploration for hydrocarbons, particularly in the USSR. The common procedures of data processing also consist of 1-D inversions of transient emf's due to the time derivative of the vertical magnetic field. The plotting point of the measurement was taken to be the center of the array in the USSR (Bernstein et al, 1977), and below the receiver in the U.S. (Keller et al, 1984).

The data acquired with the grounded line transmitters could not be inverted by 1-D algorithms, such as those initially described by Anderson (1979) and Inman (1975) to produce a geoelectric section consistent with known geology. Many of the stations showed distorted behavior, such as a change of sign in the z-component. The observation that a grounded line transmitter maximizes the influence of 2-D structures, is consistent with the results from physical modeling investigations of Wilt (1991). Also, in this test survey the geometrical layout of the grounded wire with respect to the profile line was chosen to maximize the response of the 2-D structure. This response becomes a distortion when layered models are considered.

Not only did the 1-D inversions of grounded line data result in severely distorted 1-D geoelectric sections, but the results were also highly dependent on the position of the transmitter with respect to the structure. If 1-D interpretation of the grounded line data were an objective, the field layout would have been completely different.

2.7 Information about Geologic Structure Contained in Horizontal Field Measurements

In the present practice of TEM soundings mainly the transient emf's due to the vertical magnetic field are employed. Algorithms for use of horizontal field data in 1-D inversions are not available. Part of the reason for not collecting horizontal field data in the past is the difficulty in constructing air coil receivers of large effective area (> 1,000 m^2) for making horizontal field measurements. In this survey horizontal field measurements were made with air coil receivers with effective area of 1,000 m^2 and smaller.

It is readily evident from horizontal field data that they contain important information about location of Basin and Range faults. Changes in amplitude and direction appear to occur over the known locations of the Basin and Range fault.

Again, similar conclusions were derived by Wilt (1991) from physical modeling. Over relatively, simple structure, he derived practical, empirical procedures for deriving information about structure locations from horizontal field data.

2.8 Conclusions

By comparing the geoelectric sections derived from available 1-D inversion and 1-D imaging algorithms with known geology, the following conclusions can be drawn about the utility and limitations of 1-D inversions and imaging algorithms in mapping 2-D geologic sections:

1) From the geoelectric sections produced from 1-D inversions and 1-D imaging of the vertical magnetic field data from non-grounded square transmitter loops, the 2-D structure is clearly recognized and can be approximately positioned. The absolute values of resistivity near the fault generally do not correspond with available knowledge, so that determining the depth to formations becomes subjective. For example, an arbitrary resistivity contour must be selected to represent the interface between Tertiary valley fill and Paleozoic rocks.

2) The geoelectric section derived from 1-D inversion of transient emf's due to the vertical component of the magnetic field in the center of the loop using non-grounded transmitter loops shows a geoelectric section with phantom features not related to known geology, such as layer of low resistivity within the Paleozoics on the west end of the transect.

3) The geoelectric section derived from 1-D inversions of transient emf's due to the vertical magnetic field component of grounded line transmitters does not correspond to the known geologic section. However, the survey layout was chosen to maximize the influence of 2-D structures. Thus, the 2-D structural information content of the grounded wire data appears to be greater than for non-grounded loops.

4) 1-D inversion and 1-D imaging algorithms presently only make use of transient emf's due to the vertical magnetic field. It is evident from the acquired data set that important information about fault locations is contained in horizontal field data.

In present practices of TEM for hydrocarbon reservoir exploration and development measurements are made at low station density, and 1-D inversion and 1-D imaging will remain important procedures for TEM data processing and interpretation. Effective use of 3-D fields over 2-D structures will require high station density. The geoelectric sections derived from 1-D inversion and 1-D imaging of the transient emf's due to the vertical magnetic field using non-grounded loop transmitters have limitations, but for reconnaissance exploration they yield useable geoelectric sections.

The vertical magnetic field due to grounded line transmitters responded quite strongly to the 2-D structure. The survey layout over the test site was chosen to maximize the influence of the structure, and a completely different survey design would have been used if 1-D interpretations of grounded line data were desired.

3.0 FINITE ELEMENT FORWARD MODELING

3.1 Introduction

The path of the research chosen for the modelling of three-dimensional (3-D) transient electromagnetic fields over a 2-D earth model was that of frequency domain finite element modeling with Fourier transformation to the time-domain. If we assume the x-direction to be the direction of strike, then the resistivity of the earth is allowed to vary in y and z, with the z-axis pointing downwards. The field components parallel to strike, namely H_x and E_x, can be used as potentials. Thus, the problem becomes similar to the magnetotelluric (plane wave) 2-D problem (see, for example, Wannamaker and Stodt, 1987), except that the problem must be solved for several values of the wave number, k_x, and both E_x and H_x must be solved for simultaneously because they are coupled. In the magnetotelluric case, these form independent modes because the problem is strictly 2-D and k_x is equal to 0.

The finite element method was chosen instead of integral equation methods because of the need for complete flexibility in generating 2-D models to simulate structural targets. Although integral equation methods can be more accurate and less computationally intensive than finite element methods for certain classes of models (e.g. confined bodies), it is impossible to model certain other classes of models with these methods. Any model in which the left side differs from the right side (e.g. two quarter spaces or other fault-like models) is virtually impossible to model because of the large number of cells required.

This approach was first used by Stoyer and Greenfield (1976), for frequency domain fields. They used a finite difference approach based on the transmission line analogy, following the example of Swift (1971), who used a similar method for the magnetotelluric and TURAM problem. Valla (1991) and Hohmann (1992) both used E_x and H_x as potentials, but used a quadratic basis function for the triangular elements. Valla does not report time-domain results, but does show results for a large finite loop with H_y and H_z measurements. Hohmann does not feel his code is working properly in the frequency domain at present. Lee and Morrison (1985) used a finite element method in which the secondary electric fields (three components) are the potentials. This method has an added complexity in that the electric field components perpendicular to strike (E_y and E_z) are discontinuous across resistivity boundaries. In addition, the calculation of secondary fields *only* requires the calculation of the primary field for some homogeneous or stratified model at every node in the mesh. For structural problems in which the resistivity structure of the ground can become quite complex, it was decided that the total fields should be calculated instead.

The solution developed for the finite element 2-D electromagnetic modeling problem has its roots in the work of several previous authors. As already mentioned, the use of E_x and H_x as potentials was originally used by Stoyer and Greenfield (1976). The use of "isoparametric" finite elements (in which each rectangle is split into four triangles with different resistivities) was used by Wannamaker and Stodt (1987). The finite element formulation using the Lagrange density was taken from Rodi (1976), as was the means of calculating partial derivatives needed to derive the other four field components from the E_x and H_x potentials.

3.2 Changes in Research Direction of the Program

The development of the finite element code turned out to be considerably more difficult than originally thought. The chosen field project needed to be represented by a model which could not be handled by the previously available numerical modeling code. This original integral equation modeling code is restricted to 3-D confined body models and the chosen study area required a model which was closer to a two quarter space model. Difficulties were encountered in the calculation of the final desired field components from the finite element code, especially in the vicinity of the source and more correctly in the *plane* of the source. It appears, especially after talking with other researchers working on similar problems (notably Valla, 1991 and Hohmann, 1992) that the calculation of accurate H_z fields is more difficult than originally thought. Emphasis was therefore shifted to producing results in terms of subsurface currents, which were required for the imaging scheme. These are converted by integration by the imaging software into vertical and horizontal (H_z and H_y) field components.

3.3 Formulation

The formulation of the problem begins with Maxwell's equations. Assuming harmonic time dependence of $\exp(j\omega t)$ and defining the conductivity ,σ as the inverse of the resistivity, ρ, we write Maxwell's equations as

$$\nabla \times \boldsymbol{H} = \sigma \boldsymbol{E} + \boldsymbol{J} \qquad (1)$$

$$\nabla \times \boldsymbol{E} = -j\omega\mu \boldsymbol{H} - j\omega\mu \boldsymbol{M} \qquad (2)$$

If we write these equations in the k_x domain (assuming $\exp(jk_x x)$ space dependence) and abbreviate partial derivatives, then derivatives appear as

$$\frac{\partial}{\partial_x} \rightarrow jk_x \tag{3}$$

$$\frac{\partial}{\partial_y} \rightarrow \partial_y \tag{4}$$

$$\frac{\partial}{\partial_z} \rightarrow \partial_z \tag{5}$$

After some manipulation, a pair of equations can be written so that only E_x and H_x appear as potentials and all other terms are source terms:

$$\partial_y\left[\frac{-ik_x}{p^2}\partial_z H_x\right] - \partial_y\left[\frac{k^2}{p^2}\partial_y E_x\right] + \partial_z\left[\frac{ik_x}{p^2}\partial_y H_x\right] - \partial_z\left[\frac{k^2}{p^2}\partial_z E_x\right] = -k^2 E_x + R_E \tag{6}$$

$$\partial_y\left[\frac{-ik_x}{p^2}\partial_y H_x\right] - \partial_y\left[\frac{k^2}{p^2}\partial_z E_x\right] + \partial_z\left[\frac{ik_x}{p^2}\partial_z H_x\right] - \partial_z\left[\frac{k^2}{p^2}\partial_y E_x\right] = -k^2 H_x + R_H \tag{7}$$

here, R_E and R_H are source terms, the potentials are $E_x(k_x,y,z)$ and $H_x(k_x,y,z)$ and p is given by

$$p^2 = k_x^2 + k^2 \tag{8}$$

where (assuming displacement currents are negligible) $k^2 = -j\omega\mu\sigma$.

After laborious derivation, the Lagrangian density for the system of equations can be written in the following form:

$$\begin{aligned} 2L_D = {} & \frac{1}{2}(\partial_y E_x)^2 + (\partial_z E_x)^2 + k^2 E_x^2 \\ & + \frac{1}{p^2}(\partial_y H_x + ik_x \partial_z E_x)^2 + \frac{1}{p^2}(\partial_y H_x - ik_x \partial_z E_x)^2 + H_x^2 \end{aligned} \tag{9}$$

When substituted into the Euler-Lagrange equation pair

$$\frac{\partial}{\partial y}\frac{\partial L}{\partial(\partial_y E_x)} + \frac{\partial}{\partial z}\frac{\partial L}{\partial(\partial_z E_x)} = \frac{\partial L}{\partial E_x} \tag{10}$$

$$\frac{\partial}{\partial y}\frac{\partial L}{\partial(\partial_y H_x)} + \frac{\partial}{\partial z}\frac{\partial L}{\partial(\partial_z H_x)} - \frac{\partial L}{\partial H_x} \qquad (11)$$

we get back the original equations (6) and (7).

The numerical solution for the E_x and H_x potentials is generated by specifying a grid which encompasses the region of interest and the air above it. E_x and H_x are specified (but as yet unknown) at each node of the grid. The value of E_x or H_x at the center of each element (or cell) is defined as the average of the four corner values. Within each of the four triangles which make up the rectangular element, the values of E_x or H_x are specified by a linear interpolator. The Lagrange density, specified in terms of E_x and H_x is integrated over the entire mesh to form the Lagrangian. Added to this are boundary condition contributions from integrals around the edge of the mesh. We then take the partial derivative of the total Lagrangian with respect to each of the unknown values of E_x and H_x and set these equal to zero. This forms a matrix equation in the unknowns. Known (source) terms are moved to the right-hand side to form a matrix equation as

$$[A]\bar{x} = \bar{s} \qquad (12)$$

If there are n nodes in the vertical direction and m nodes in the horizontal direction, the dimension of the system of simultaneous equations is 2nm, and all values are complex. This system of equations is generated and solved for several values of k_x and several values of ω. For each solution, the E_x and H_x field components are used to generate the other four components (E_y, E_z, H_y and H_z) as desired. Two Fourier transforms are carried out, one from the wave number (k_x) domain to the space (x) domain and one from the frequency domain to the time domain. These are carried out for each of the desired field components.

One of the major problems in the implementation of finite element solutions of this type is the calculation of additional components (E_y, E_z, H_y and H_z) from the E_x and H_x potentials. Normally, this is carried out using some sort of numerical differencing to calculate partial derivatives of E_x and H_x and substituting these into Maxwell's equations to calculate the field component. Often the accuracy of these derivatives is much less than the accuracy of the potentials themselves, and the combination of two derivatives leads to a very inaccurate field value.

In this work, we followed the suggestion of Rodi (1976) and constructed a second Lagrangian and constructed and solved a second finite element problem for the horizontal field components (E_y and H_y).

Horizontal derivatives can be accurately calculated (e. g. using a spline function) and these are used as needed to calculate the vertical field component, especially H_z.

Because the formulation was designed for *source free regions*, the calculation of H_z was not successful in the vicinity of sources. This will have to be reformulated to account for sources.

3.4 Numerical Computations

Numerical computations were carried out on a MicroWay Number-Smasher 860 board running at 33 MHz with 8 Mb of RAM memory. This board was fitted into an ALR Power VEISA with a 33 MHz 386 processor, 64 Kb cache, 5 Mb of RAM memory and a 100 Mb hard disk. The software used to perform the calculations was written using FORTRAN 77 for the majority of the code. Assembly language was used to perform the vector operations needed in the LU decomposition and back substitution process for solving the simultaneous equations.

The Intel i860 processor carries the nickname "Cray on a chip" and is a RISC type architecture. The processor features pipelining, so that, given the right kind of problem and carefully hand coding, it is capable of producing one integer and two floating point operations with each clock cycle. We were not able to make full use of its potential 60 MFLOPS (million floating point operations per second) capability, due to lack of time and expertise in i860 assembly language programming.

All runs were carried out using a 200 m square finite loop with receiver stations located every 100 m from 1300 m to the left of the loop to 1300 m to the right of the loop. Grid elements within the main part of the grid were 25 m wide. The finite loop was simulated by placing a vertical magnetic dipole at every node within the area defined by the 200 m wide loop (including at the loop edges) and integrating the results numerically in the x direction. The loop is always centered at x=0, so stations are situated from -1300 m to +1300 m.

Mesh size was 36 (vertical) by 169 (horizontal) nodes, with 9 of the vertical nodes in the air above a flat earth. This represents a complex matrix which is 12,168 by 12,168. 24 wave numbers (k_x-values) were used and 42 frequencies were used. Frequencies ranged from $1.8 \cdot 10^{-4}$ to 10,000 Hz, with 6 points per decade over most of the range. Wave numbers included 0 and ranged from 0.2 to 1280 m^{-1}. Each model run took 12 hours, or 43 seconds per point in wavenumber and frequency. Computation time should

be proportional to the number of horizontal nodes and to the cube of the number of vertical nodes. Computation time is also proportional to the number of wave numbers times the number of frequencies.

The combined processor and software was running at an estimated 9 MFLOPS. All calculations were carried out in single precision, using a 32-bit IEEE floating point format. It is estimated that more careful hand coding of the vector operations would result in a speed increase of three to six times.

3.5 Results

We believe, as is shown in the following sections, that the basic results from the finite element modeling are correct. Surface based H_z fields were not good in the vicinity of the source, due to the fact that the algorithm (adapted from Rodi, 1976) was designed for source-free regions. On a flat earth with a finite dimension loop source, the row of elements including the receivers also includes the source. This renders the algorithm in its present form unusable. Additional theoretical work must be carried out to deal with calculations of fields in regions which contain the source, or integral, rather than differential, methods might be better at deriving these desired field components.

Two other groups (Valla, 1991 and Hohmann, personal communication, 1992) have attempted to implement a similar finite element approach and have had difficulty with the formulation presented here (this was only realized after our work had been completed). In both cases, they used a quadratic, rather than a linear, representation for the basis functions. At last report (Hohmann, 1992), the formulation was still suspect, partially due to coding problems but theoretical considerations were not completely satisfied either. In our formulation, the E_x field is not actually used as a potential; instead, $E_x/j\ldots$ was used as a potential, which we believe makes the solution much more stable, especially at low frequencies (Hohmann had difficulty only with low frequencies and Valla did not attempt to consider low frequencies, since he was working in the frequency domain).

3.6 Tests of Accuracy

Although tests of accuracy were periodically carried out during the development of the finite element code, most of these were qualitative and the results are not in presentable form. True tests of accuracy are virtually impossible, since there is not a working 2.5-D time domain modeling code for comparison. We know that there are problems with the calculation of the most desired field component, H_z, and we know what work has to be done to solve this problem. The accuracy for the finite element

method was tested by comparing x-directed (x is the strike direction) currents in the source-receiver plane to analytical calculations for a homogeneous earth of 15 ohm-m.

Frequency domain comparisons indicated an error between the numerical and analytical results on the order of one to two percent. Time domain results are presented here in graphical form for comparison. Figure 14 shows the contour map of current distribution in the subsurface of a 15 ohm-m half space calculated by analytical means. Figure 15 shows the same currents calculated by the numerical (finite element) method. Note that the two figures for times of 89 μsec and are much the same. One difference lies in the fact that the analytical results (Figure 14) extend further in the y-direction (left-right) than the numerical results (Figure 15). Also, there is more structure and some difference near the surface and the source; this is due to the fact that the numerical results start at zero depth (plotted at 12.5 m depth) while the analytical results start at 25 m depth. In addition, the numerical results are expected to be less accurate near the source. The third difference is in the deep structure of the currents under the source. For such an early time gate, both the analytical and the numerical calculations are not expected to be accurate below about 100 m depth. The depth to which the calculations are valid increases with time. Overall, the comparison is quite good.

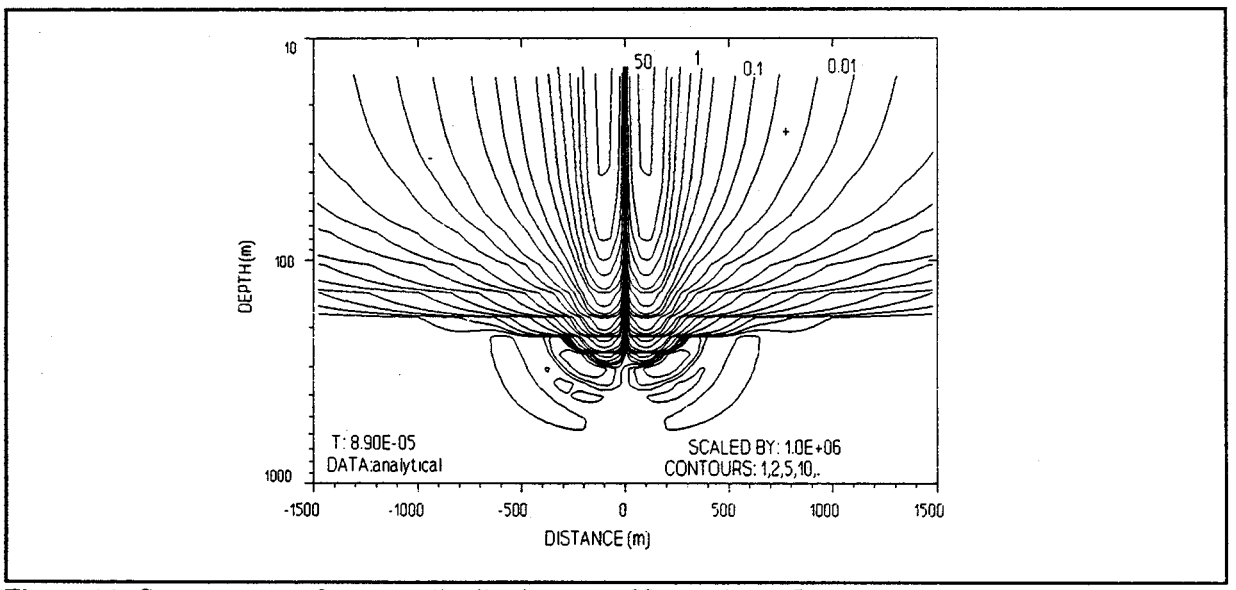

Figure 14. Contour map of current distribution at t=89 μsec in a 15 ohm-m homogeneous half space. Contours are placed at intervals of 1,2,5,10,... All values are scaled upwards before plotting by a factor of 10^6.

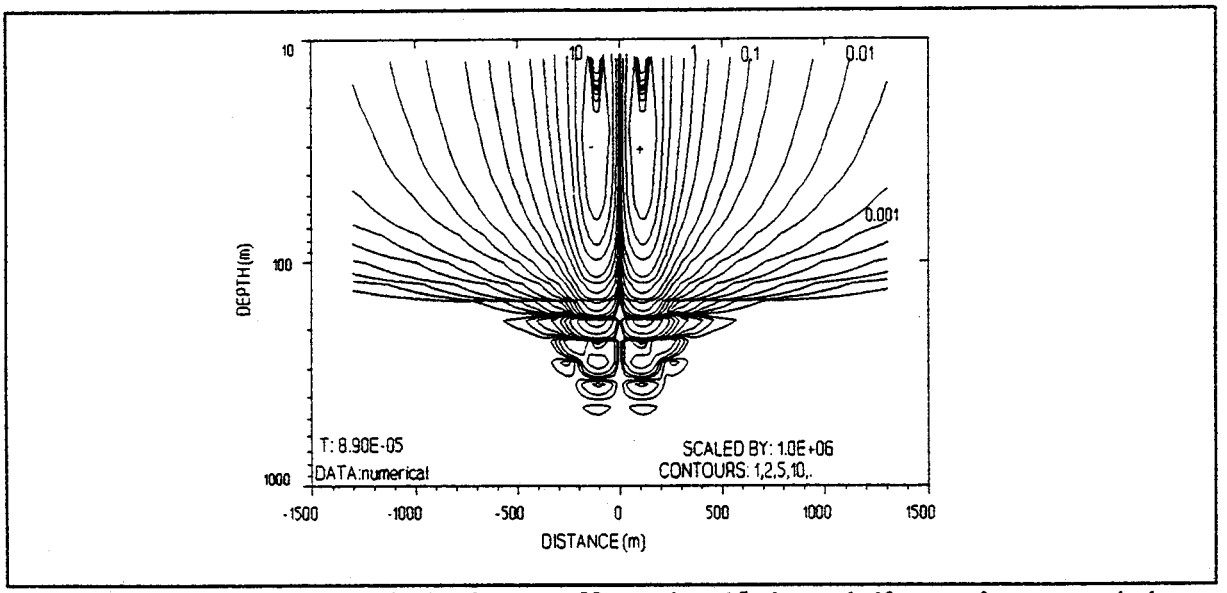

Figure 15. Contours of current distribution at t=89 μsec in a 15 ohm-m half space, from numerical modeling. Contours are placed at 1,2,5,10,... All values are scaled upwards before plotting by a factor of 10^6.

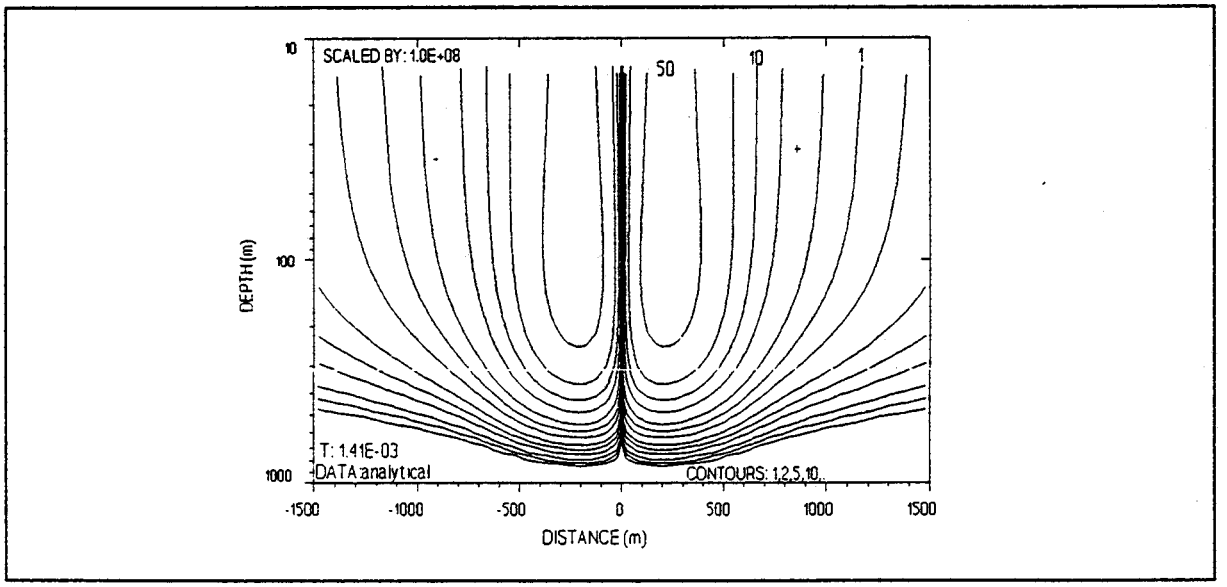

Figure 16. Contour map of current distribution from analytical calculations at t=1.41 msec. All values are scaled upwards before plotting by a factor of 10^8.

The next two figures show the comparison between the analytical (Figure 16) and the numerical (Figure 17) results at a later time of 1.41 msec. The comparison between the numerical and the analytic results is similar to that shown for Figures 14 and 15.

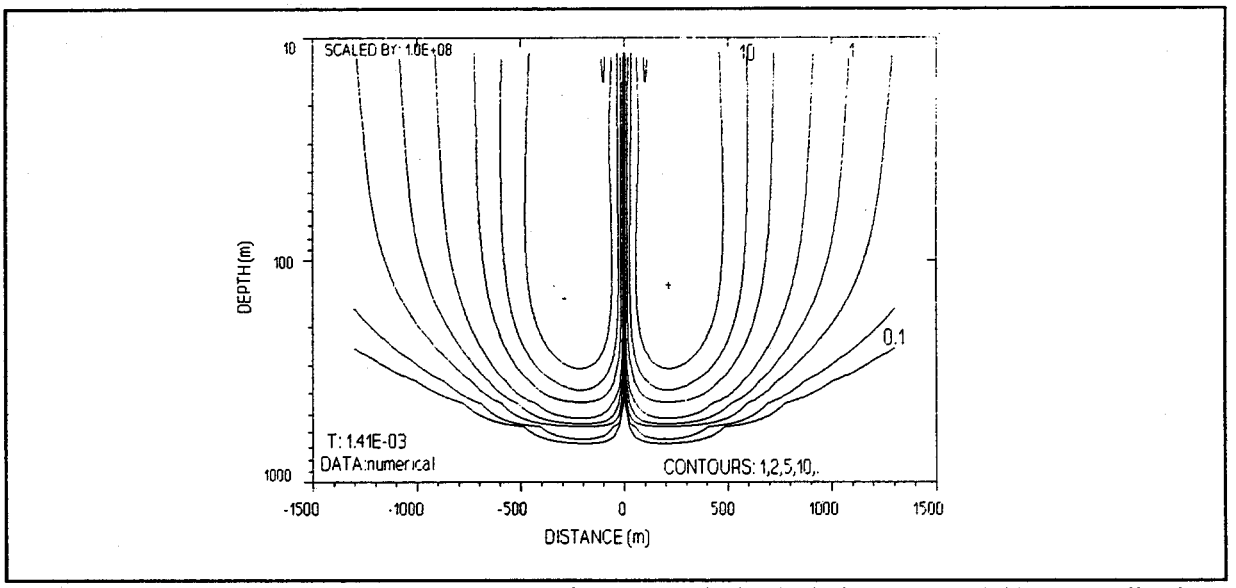

Figure 17. Contour map of current distribution from numerical calculations at t = 1.41 msec. All values are scaled upwards before plotting by 10^8.

3.7 Use of Results in Imaging of TEM Data

One unexpected outcome of the project is that the TEM imaging scheme, which up to now had used a 3-D modeling program to assist in the performance of the imaging, required a 2-D modeling package because of the inability of the 3-D scheme to handle the required model. The problem is that the area chosen for the field project was a fault, similar to a two quarter space structure which cannot be handled by the 3-D modeling code, which is designed for confined bodies. Thus it was imperative that the currents used as a basis for the imaging scheme be calculated from the finite element program, which is the only code available for such models. This offsets the fact that not enough time and resources were available to complete the finite element code to the point of generating H_z field component data.

Figure 18 shows the current distribution for a two quarter space model with 100 ohm-m material on the left and 12 ohm-m material on the right at 85 μsec. The model is shown in Figure 19. At 1.41 msec, the current distribution is as shown in Figure 20. Note that the currents in the resistive quarter space are much lower than those in the conductive one and that they decay and diffuse much more rapidly. These calculations were used in the second iteration of the imaging.

Figure 21 shows the model used in the third and final iteration of the imaging. This is very close to what is believed to be the structure at the field site. Figures 22 and 23 show the current distribution at times of 85 μsec and 1.41 msec. Note that the 40 ohm-m surface layer is evident by the slowing of the

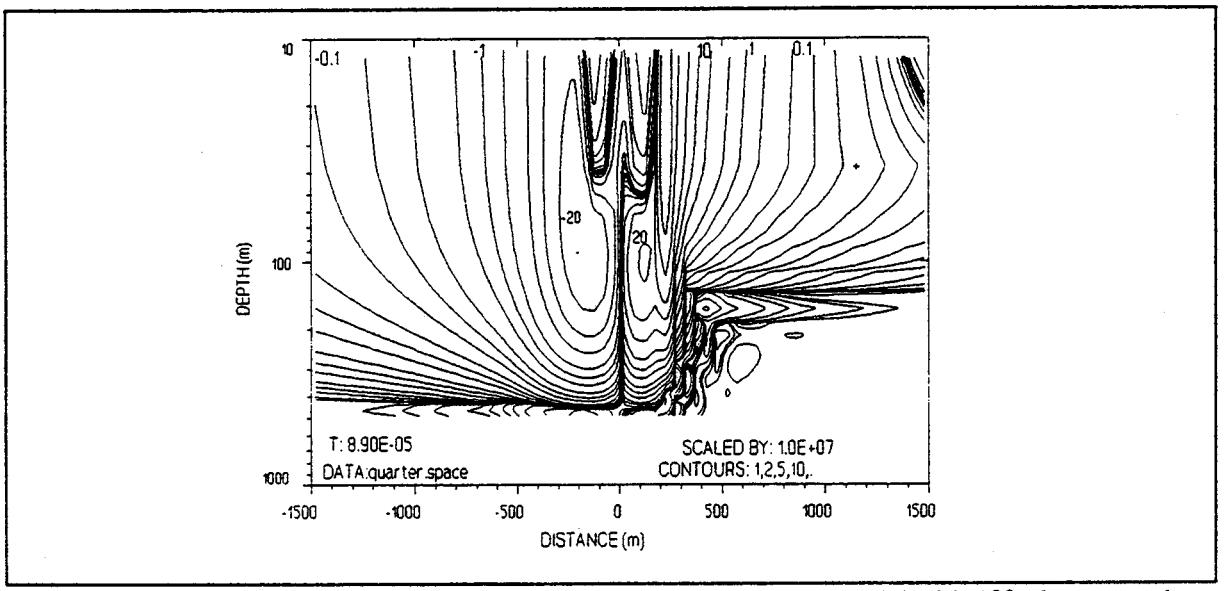

Figure 18. Contour map of current distribution for a two quarter space model with 100 ohm-m on the left and 12 ohm-m on the right from numerical computation. Separation is at 200 m.

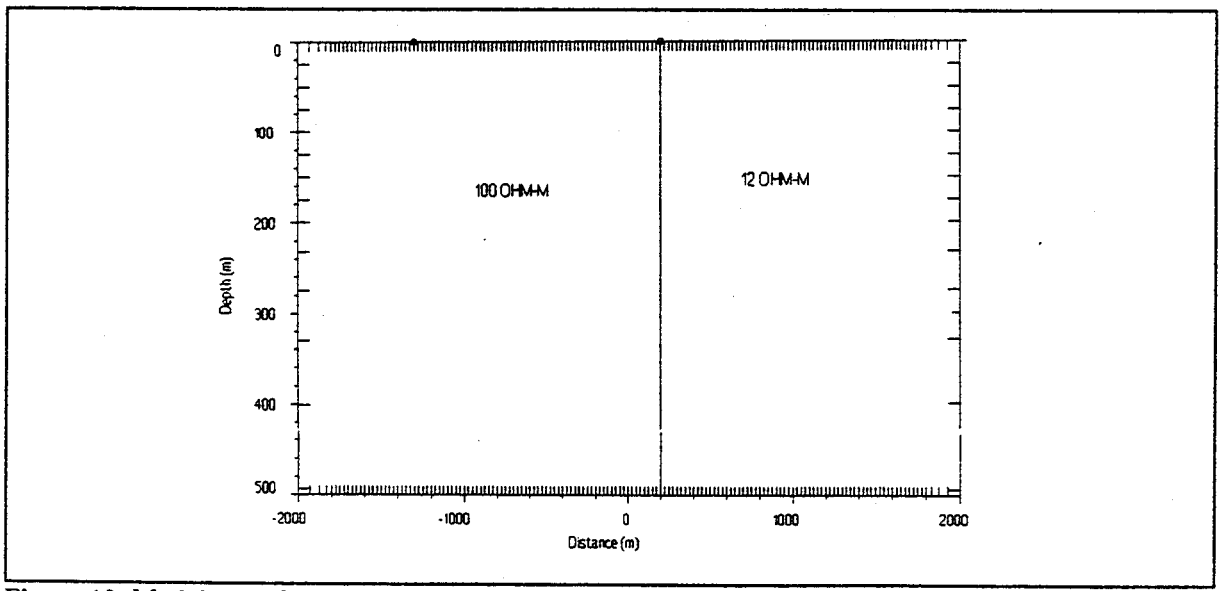

Figure 19. Model used for two quarter space calculation. Flat lying 200 m square loop source is at center of model.

current movement on the left and the increase in the current movement on the right. For the 1.41 msec data, the small 5 ohm-m conductor is evident at 40 m depth and -200 m distance. The fault block is also evident near 250 m depth from -200 to 300 m distance.

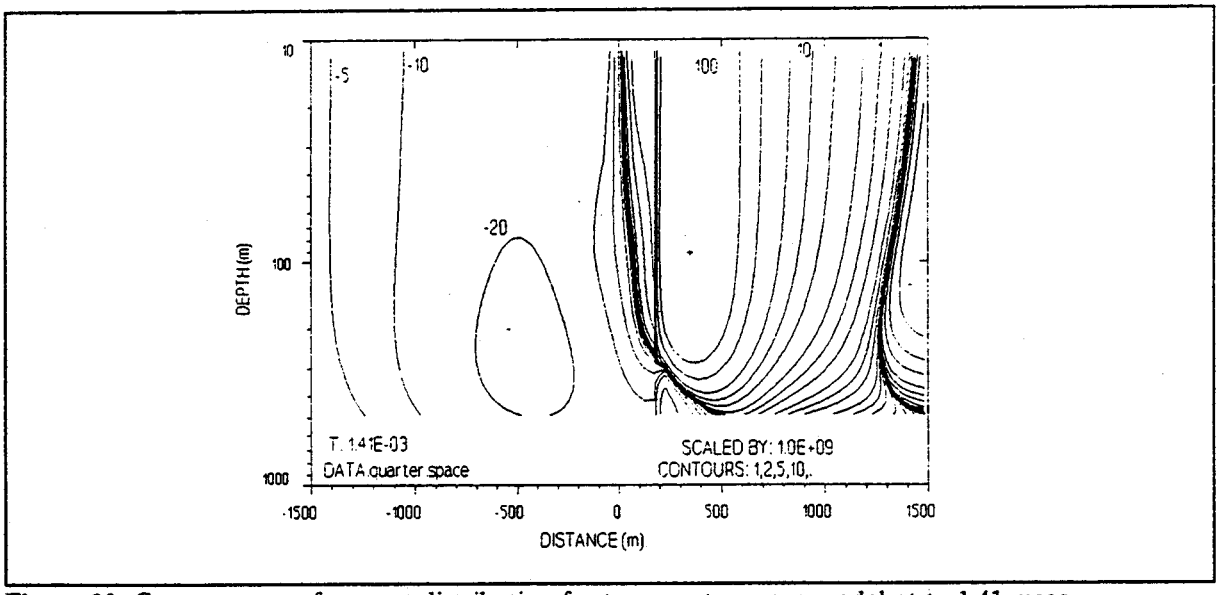

Figure 20. Contour map of current distribution for two quarter space model at t=1.41 msec.

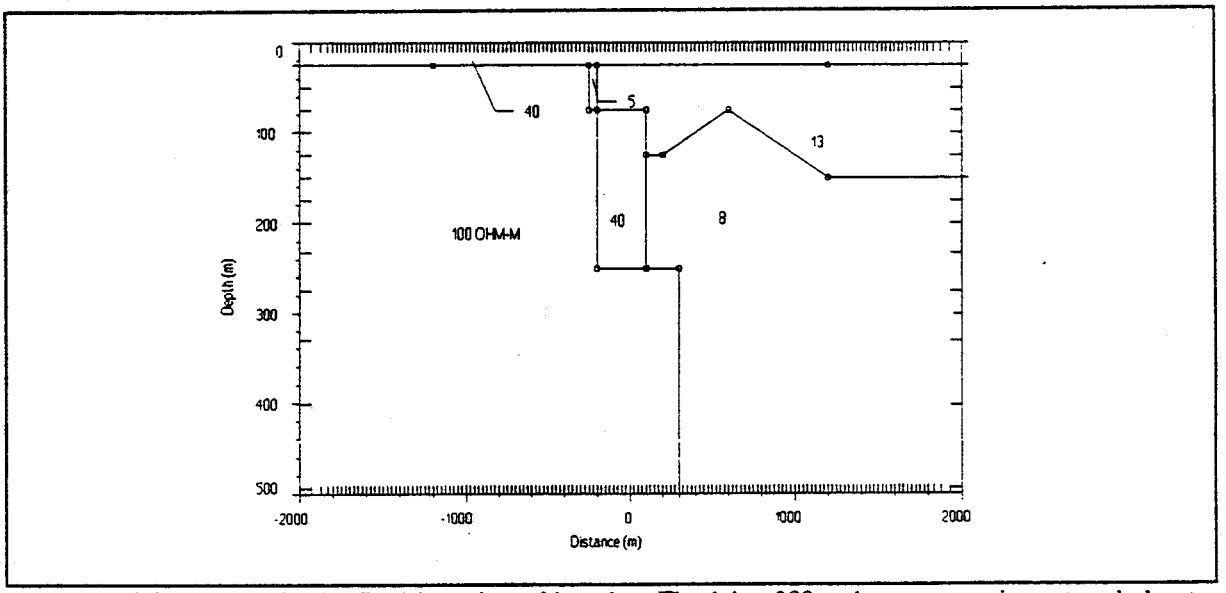

Figure 21. Model used in the final iteration of imaging. Flat lying 200 m loop source is centered about 0.0.

3.8 Summary and Conclusions

The development, implementation and verification of the finite element scheme for 3-D time domain electromagnetic fields over a 2-D earth turned out to be considerably more difficult than originally expected. Acquisition of a Microway Number-Smasher 860 processor board was required even to bring the project to the present state of completion. Although further development is required to be able to model measured fields on the earth surface for a finite loop source, the finite element modeling scheme turned

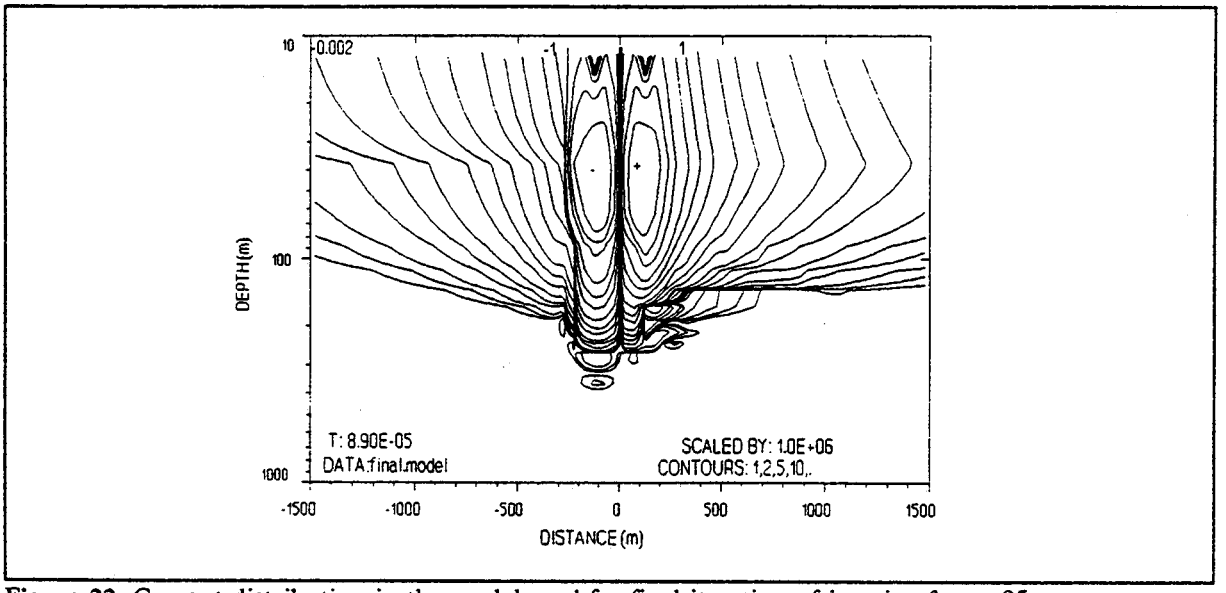

Figure 22. Current distribution in the model used for final iteration of imaging for t=85 μsec.

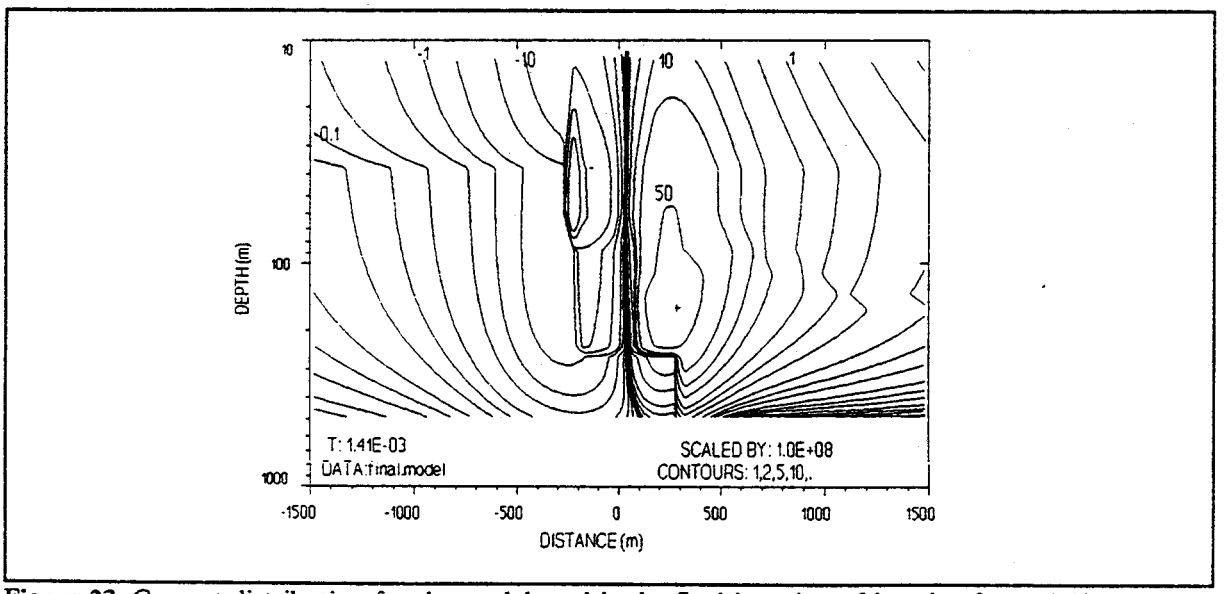

Figure 23. Current distribution for the model used in the final iteration of imaging for t=1.41 msec.

out to be most valuable as a support tool for the imaging, to the extent that the imaging for the 2-D structure chosen for this project would have been impossible without it.

Verification of accuracy was limited to comparison with analytical results for the current in the strike direction at y=0 inside a homogeneous earth. Only the current in the strike direction at y=0 was used in the imaging part of the project. The results of the imaging of the field data produced a reasonable and seemingly correct result, given the additional information which was available for the project area.

The modeling scheme appears, at present, not economically viable, since it requires about 12 hours of CPU time on a 9 MFLOP machine to perform the calculations. As computer equipment becomes more powerful and the needs of the industry for these type of modeling results become greater, this situation will improve.

4.0 TEM 2-D SUBSURFACE IMAGING

4.1 Introduction

The forward modeling of 3-D EM fields over 2-D structures described in Section 3 has as its objective to predict EM field behavior over 2-D structures. The computation process was shown to be computer resource intensive and for some time will not readily lend itself to incorporation in inversion routines, or rapid iterative forward modeling to obtain matches with observed data. The imaging process described in this section on the other hand, is designed to image current flow patterns and arrive at an approximation of the 2-D structure. Subsequently, forward models can be computed by the algorithms developed in Section 3 to verify the structures derived from imaging.

In this section the physical concepts underlying the imaging method are first described, and this is followed by its use on a data set acquired over the test site in the Basin and Range in Nevada.

Traditional use of TEM for structural investigations has been to acquire profiles of central loop soundings and interpret the data using a 1-D layered earth inversion method with a discrete number of layers. The individual sounding interpretations are then spliced together into a profile to yield a subsurface structural cross-section. Recent efforts (Macnae and Lamontagne, 1987; Nekut, 1987; and Eaton and Hohmann, 1989) have led to approximation of the vertical component of the magnetic field by use of a single equivalent current filament, or a stack of a few filaments, as in the case of Macnae and Lamontagne (1987), at each measurement time, so as to arrive at a continuous resistivity-depth profile without discrete layers. Just as with the layered earth inversion approach, the individual approximate 1-D sounding interpretations are spliced together into a cross-section. The smoothly varying resistivities are contoured to produce a subsurface resistivity section. This method has become known as 1-D TEM imaging.

A basic limitation of all 1-D methods is the assumption that the field variations are related to the earth directly underneath the receiver. However, currents diffuse down and outward, so that the 1-D methods will interpret an anomalous zone directly underneath the receiver when real anomalous features may be laterally displaced. When sufficient data is acquired it is usually possible to approximately locate a feature in the correct vicinity, as was demonstrated in Section 2. In other words, 1-D methods can confirm the existence of an anomalous feature and approximately locate it, but may not provide adequate lateral resolution of the true resistivity structure (Newman and Hohmann, 1987). At present, structural

interpretations utilizing TEM data stop with this approximate 1-D-derived picture for lack of better methods of interpretation.

4.2 Imaging Method Overview

The 2-D Subsurface Imaging procedure directly interprets the vertical and horizontal components of the magnetic field into patterns of subsurface current flow. An initial current distribution is calculated as a function of time for an appropriate average or background model. Then these current distributions are modified in position, shape and amplitude to achieve an improved fit to the data. Thus, localization of current anomalies is achieved that is subsequently processed into a geoelectric section from which a structural interpretation can be inferred. This procedure also is flexible in that it can accommodate widely varying structures.

The interpreted current distributions are then stacked and ratioed to the stacked current distributions for the initial model. This ratio of interpreted to initially calculated current provides a means to estimate the resistivity structure. If the current is interpreted to increase in any subsurface element it indicates a higher conductivity. Likewise, if the current is interpreted to decrease it indicates a lower conductivity. An interpreted resistivity is assigned to every subsurface element by assuming a linear relationship between current variation and conductivity variation.
The stacking process includes weighting factors and windowing functions designed to sharpen resolution in the resulting geoelectric image.

The first requirement for implementation of this approach is data density sufficient to characterize the spatial variation of the TEM magnetic field for every transmitter position. Therefore, for the 2-D Basin and Range structure, a profile of measurements roughly perpendicular to the structural strike direction are needed, as well as measurements of vertical and horizontal components of the TEM fields. Any given transmitter position will optimally electromagnetically illuminate only certain regions of the subsurface, and to achieve complete structural illumination multiple transmitters are needed in a regularly spaced profile that yields overlapping measurement profiles. This dense, regular, redundant survey design is the basic requirement for any viable structural imaging method.

Effective TEM imaging processing can, therefore, not be applied to the low station density presently common in deep electrical exploration. It demands acquisition of high data density such as collected for the specific purpose of testing the imaging algorithms over the Basin and Range test site.

4.3 Interpretation of Current Distributions

The interpretation of the geoelectric section by the 2-D imaging method first interprets current flow in the subsurface and, since a complete current flow representation is utilized, requires a starting model.

The first step is to establish an approximate or background model that resembles the anticipated geoelectric section. This might be created from well log information, geologic data, prior analysis of other geophysical data, or even 1-D interpretation of the central loop measurements of the present survey. It might also be created from a prior 2-D imaging interpretation iteration if more than one imaging iteration is being performed on the data set. The model may be horizontally layered or 2-D.

A subsurface grid is formed and electrical current distributions are computed for this initial geoelectric model. The calculations of current distribution, as a function of time, were conducted with two types of algorithms

- the personal computer version of the 3-D TEM integral equation modeling program described by Newman et al (1986),

- the finite-element modeling program developed as part of this research project and described in Section 3.

For each individual time slice, and for each transmitter position, the calculated current distribution is modified, or perturbed, to achieve a better fit to the measured magnetic (H) fields along the profile for that transmitter. An example of the result of this process is provided in Figure 24. The H-fields along the profile are calculated from the subsurface current distribution by means of Biot-Savart's Law for an elemental volume,

$$\vec{h}(x,y,z,x',y',z') = \frac{[\vec{j}(x,y,z) \times \vec{r}]dv}{4\pi r^2}, \qquad (13)$$

and summing over all subsurface elements (x,y,z) for each receiver (x',y',z'). Each subsurface element is assumed to represent half of a current filament of an amplitude equal to the amplitude of the current in the element and a shape identical to the shape of the transmitter loop. Representation of half a filament is used because there is another element on the other side of the transmitter (or the other side of the

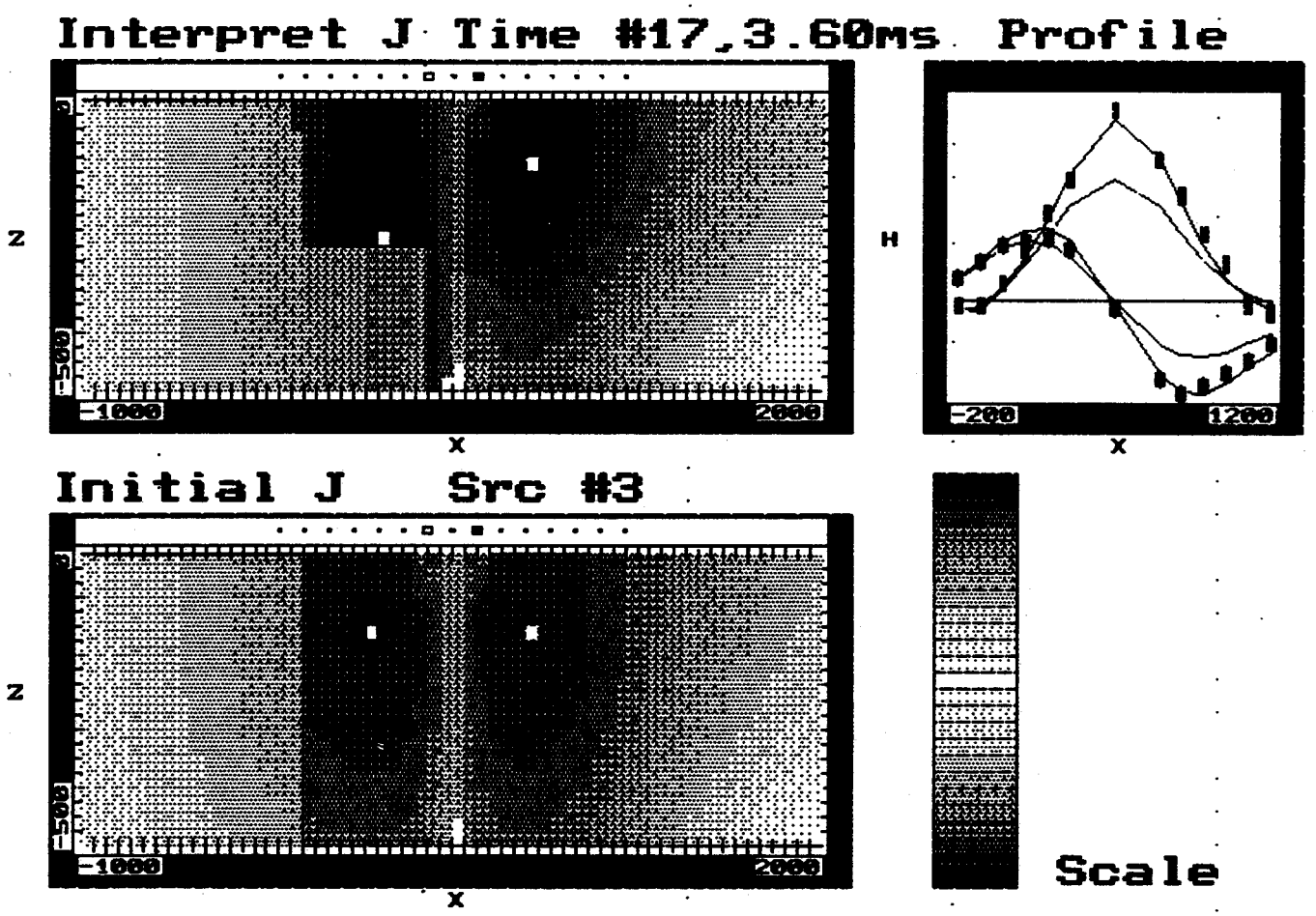

Figure 24 An example of the process of interpreting the current distribution for one time slice and one source position. The upper plot is the interpreted current distribution. The lower plot is the starting current distribution. The profile viewport displays the x- and z-component profiles. The best fit lines are the profiles for the interpreted current section. The misfit lines are the profiles for the starting current section. The discrete points are the measurements along the profile. The horizontal line provides a reference to zero amplitude. The highest amplitude profile is the z-component and the other profile is the x-component. The amplitude scale for the current density is a floating scale pegged to the highest amplitude in the section. There are two contour intervals per decade of amplitude. Vertical exaggeration is 2.4:1.

amplitude crossover) to represent the other half. Each half filament is then discretized and integrated to yield the contribution to the magnetic field from that element. Figure 25 displays the various geometrical relationships involved in this calculation.

The computations were verified by comparing them to magnetic fields calculated by numerical algorithms for both layered earth and elongated 3-D structures. These comparisons displayed agreements within a few percent, except at very early or late times where the error may increase toward 10 percent or slightly more. The early time error is caused by the coarseness of the grid near the transmitter while the late time error is caused by the grid not extending far enough out to encompass all of the significant current flow at these late times.

Successive iterations on the current distributions gradually bring the calculated magnetic field profiles into a least-squares best fit with the measured magnetic field profiles. Modifications are made until all time slices for all transmitters have achieved their best fit. In adjusting current distributions care is taken to preserve integrity and consistency with the physics of current diffusion. The objective of the process is to arrive at current distributions that would be similar to those computed by forward models for the geoelectric section, and it further illustrates the importance of having a finite element forward modeling capability used in conjunction with the imaging process.

4.4 Construction of Image Resistivity Section

The present results are time-varying current distributions in the subsurface that are consistent with the H-fields measured at the surface. However, the objectives of any exploration program is not to calculate current distributions, but to produce a geologic section. The next step, therefore, is to obtain a geoelectric section from the current distributions from which geologic structure may be inferred.

For all practical purposes current flows essentially everywhere in the subsurface at all times, and in each zone there is a correlation between amplitude of the current and resistivity. However, the contribution of current flow in each subsurface element to the H-fields measured at the surface changes over time and with electromagnetic illumination. Therefore, the objective is to define for each subsurface zone the window of time during which current flow within that zone has significant influence on the measured data and, in particular, significant correlation to the resistivity of that zone. However, it is also true that the absolute current flow within any particular zone is not just a function of that zone's resistivity, but is also a function of the current flow in, and resistivity of, a considerable volume of

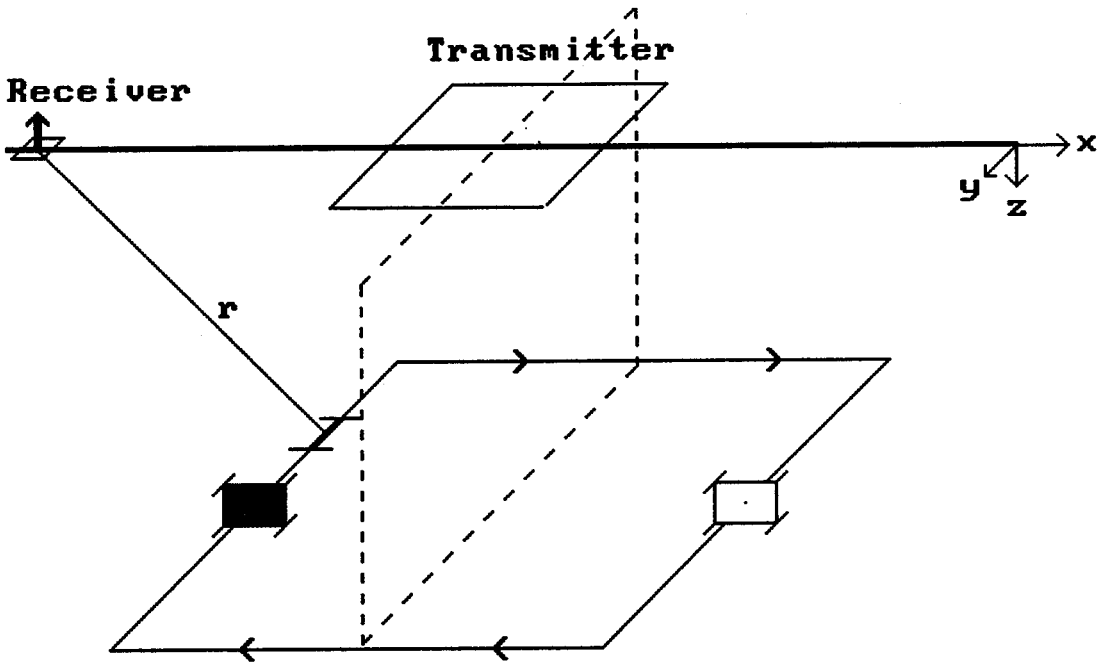

Figure 25 Depiction of the method of integrating around one current filament to calculate the magnetic field at one measurement location using Biot-Savart's Law. Each half filament is assigned the current density calculated for the element on that side of the source center position.

surrounding host rock. This interdependence is what inherently limits resolution in EM and makes development of an imaging procedure difficult.

Next, the rationales behind selecting time windows for the stacking of each subsurface element are described. Further detail on this process is given by James (1990). The current flow at very early times is essentially an image of the transmitter. As diffusion proceeds the zones of maximum current flow move down and outward. This zone of high current flow also expands with increasing time. Therefore the zone of significant "illumination" of the subsurface for the entire range of time approximately looks like a hollow cone. Zones at low or high angles from vertical, relative to the transmitter position, lie outside this zone of significant illumination. On the other hand, such zones may lie within the zone of significant illumination for an adjacent transmitter, illustrating the need for multiple sources and receivers for 2-D mapping. In addition, the illumination pattern is strongly governed by the geoelectric section. For example, the block fault structure present at the test site causes significant distortion to the pattern of current flow; current intensity is low in the Paleozoic rocks over the Range and high in the Tertiary valley fill of the Basin.

Criteria used for including pixels in the stacking and weighting process are:

1) The time window for each pixel is selected so that the beginning of the window includes the time of maximum current, and continues to later time gates to include the time of greatest relative contribution of the current in that pixel. Here relative contribution refers to the contribution from that element in proportion to the entire contribution from the discretized subsurface for an individual time slice.

2) Pixels with high current intensities are weighted more strongly because they are more strongly correlated with the resistivity of that local zone of the subsurface than are pixels of weaker currents. The position of high current intensities in the subsurface is clearly a function of both time and geoelectric section.

The process is illustrated in Figure 26 where, for the Basin and Range structure, the weighting (or contribution) of each pixel is given above, and contours of current intensity below at a time of 1.1 msec. Also shown on each is the assumed geologic model for the initial calculations. This figure illustrates several aspects discussed above:

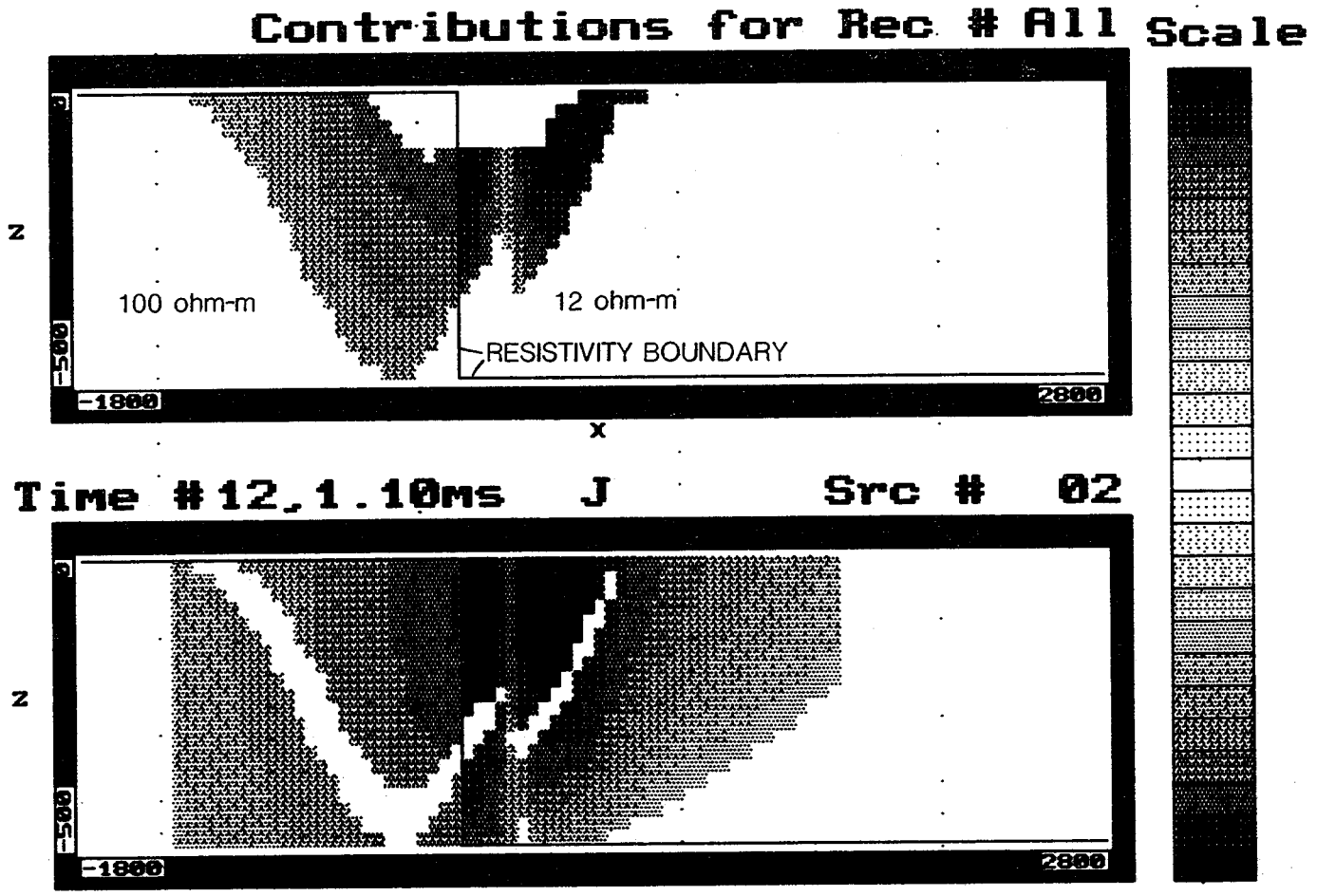

Figure 26 An example of a 'contribution' section (upper) with its corresponding current section (lower). The white pixels on the lower plot interior to the current distribution show the location of all elements for which the current is at its maximum, as a function of time, in that element. The time of maximum current in any one element is well in advance of the time of the maximum relative contribution of the current within that element. (The position of the maximum current at any one time is closer to the source than the trace of elements at their maximum current with respect to time). Vertical exaggeration is 2.6:1.

1) The large influence of the geoelectric section on current intensity contours. Over the Range where Paleozoic rocks are encountered, current intensities are low. Current intensities are considerably higher over the Tertiary Valley fill. This is also reflected in the contribution section.

2) For the intermediate time slice illustrated pixels very near the transmitter loop are "turned" off, and this zone of "turn-off" advances from the transmitter with increasing time. Pixels very far from the transmitter loop are also "turned" off, and this zone of "turn-off" retreats from the transmitter with increasing time. The zone of "turn-on" expands outward from the transmitter with increasing time in a pattern and at a rate strongly governed by the geoelectric structure.

The entire process can be mathematically summarized as follows:

First the summed current in each pixel is calculated

$$J_k^i(x,z) = \sum_{t_1(x,z)}^{t_2(x,z)} j_k^i(x,z,t) \cdot \omega_k^i(x,z,t), \tag{14}$$

and

$$J_k^c(x,z) = \sum_{t_1(x,z)}^{t_2(x,z)} j_k^c(x,z,t) \cdot \omega_k^c(x,z,t), \tag{15}$$

where

$$\omega_k^i(x,z,t) = g_k^i(x,z,t) \,/\, g_k^i(x_m,z_m,t), \tag{16}$$

$$\omega_k^c(x,z,t) = g_k^c(x,z,t) \,/\, g_k^c(x_n,z_n,t), \tag{17}$$

$$g_k^i(x,z,t) = j_k^i(x,z,t) \cdot G(x,z), \tag{18}$$

$$g_k^c(x,z,t) = j_k^c(x,z,t) \cdot G(x,z), \tag{19}$$

$$G(x,z) = \sum_{l=1}^{L} \sqrt{g_x(x,z,l)^2 + g_z(x,z,l)^2}, \tag{20}$$

j is the current density, the superscript 'i' denotes that the quantity is derived from the interpreted current, the superscript 'c' denotes that the quantity is derived from the current calculated for the starting model, the subscript 'k' denotes that the quantity is for source k, g_x and g_z are calculated from (13) using a unit test current density, L is the number of receivers in a measurement profile for any one source, (x_m,z_m,t) is the position of the maximum summed contribution at time t for the interpreted current section, (x_n,z_n,t) is the position of the maximum summed contribution at time t for the current section calculated for the starting model, and $t_1(x,z)$ and $t_2(x,z)$ are the times of the beginning and end of the stacking window and are functions of position. Normally $t_1(x,z)$ corresponds to the time of maximum interpreted current flow in the element and $t_2(x,z)$ is set such that the window includes a user specified number of time gates. The number of time gates is chosen so that the time of maximum relative contribution of the element is included in the window. This time of maximum relative contribution lags the current maximum by a number of time gates that increases with distance from the transmitter. For much of the subsurface section the lag is in the range of 3 to 6 time gates.

Then the imaged resistivity for each pixel for each source k is calculated

$$\rho_k^i(x,z) = \frac{J_k^c(x,z)}{J_k^i(x,z)} \cdot \frac{W_k^i(x,z)}{W_k^c(x,z)} \cdot \rho_m(x,z), \tag{21}$$

where

$$W_k^i(x,z) = \sum_{t_1(x,z)}^{t_2(x,z)} \omega_k^i(x,z,t), \tag{22}$$

$$W_k^c(x,z) = \sum_{t_1(x,z)}^{t_2(x,z)} \omega_k^c(x,z,t), \tag{23}$$

and the subscript 'm' denotes the element's starting model resistivity. The final imaged resistivity is then

$$\rho^i(x,z) = \sum_{k=1}^{K} \rho_k^i(x,z) \cdot W_k^i(x,z) \cdot W_k^c(x,z), \tag{24}$$

where K is the number of sources along the profile.

4.5 Data Processing and Results

In this section the processing of the test data over the Basin and Range 2-D structure in Nevada and the derived geoelectric section are discussed. The processing consists of several sequential steps.

Step 1 - Deconvolution

The field data consists of voltages measured in air coil receivers due to the impulse response of the system waveforms employed in the Geonics transient systems. These voltages are deconvolved using the procedures described by Lacoste (1982).

Step 2 - Computation of Magnetic Fields by Integration of Emf's

In the acquisition voltages due to the time derivative of magnetic fields are measured. Since the interpretation method is based on comparison of magnetic field data it was necessary to then integrate the voltage measured over time to recover the magnetic field:

$$H_i(t) = \int_t^{t_0} (dH/dt)dt + H(t_0), \tag{25}$$

where i denotes the field component and t_0 is the last data time. The main difficulty lies in achieving a correct constant of integration. To design the procedure such that the integration constant is zero or negligible, the procedures described by Nekut (1987) were adopted.

In this procedure, each voltage versus time curve is extrapolated for two decades in time beyond the last measured time gate so that any remaining integration constant is negligible. Central to this extrapolation is the choice of the rate of decay versus time. The late time rate of decay is known for any layered earth for both z and x component emf data. This known rate of decay is used in the extrapolated data for the last time of extrapolation. For the earlier extrapolated points the observed decay at the end of the measured data is geometrically averaged with this known late time rate of decay to achieve a smooth curve that gradually approaches the known rate of decay. The integration process starts from the end of the extrapolated data but only the magnetic field values at measurement times are retained for imaging after integration is complete. This procedure works well but is sensitive to noise in the data in later time gates. To correct for noisy data some data points were discarded or decay slopes were modified. The resulting magnetic field values were utilized in matching with the magnetic field computed from the current distributions.

Step 3 - Iterative Imaging

In this processing step the procedures described in Sections 4.3 and 4.4 of interpreting current distributions and stacking current in each pixel to yield an image resistivity section takes place.

The process begins with forming a model for a geoelectric section of the subsurface. In practice, such models often will be based on the geoelectric section derived from 1-D interpretations. In this R&D effort several initial models were tested to evaluate convergence characteristics of the 2-D imaging method, and here the process will be illustrated on the geoelectric models shown in Figure 27. They correspond relatively closely to the known Basin and Range structure with high resistivities over the Paleozoic Range rocks, and low resistivities over the Tertiary Basin fill. The first model is a simple vertical contact model with the position of the contact located at the position of the outcrop observed in the field. The second model was created from the interpretation of the imaging section for the first model. The models utilized were intentionally constrained to horizontal and vertical boundaries used to define the fault structures in order to limit the range of structural testing for this exercise.

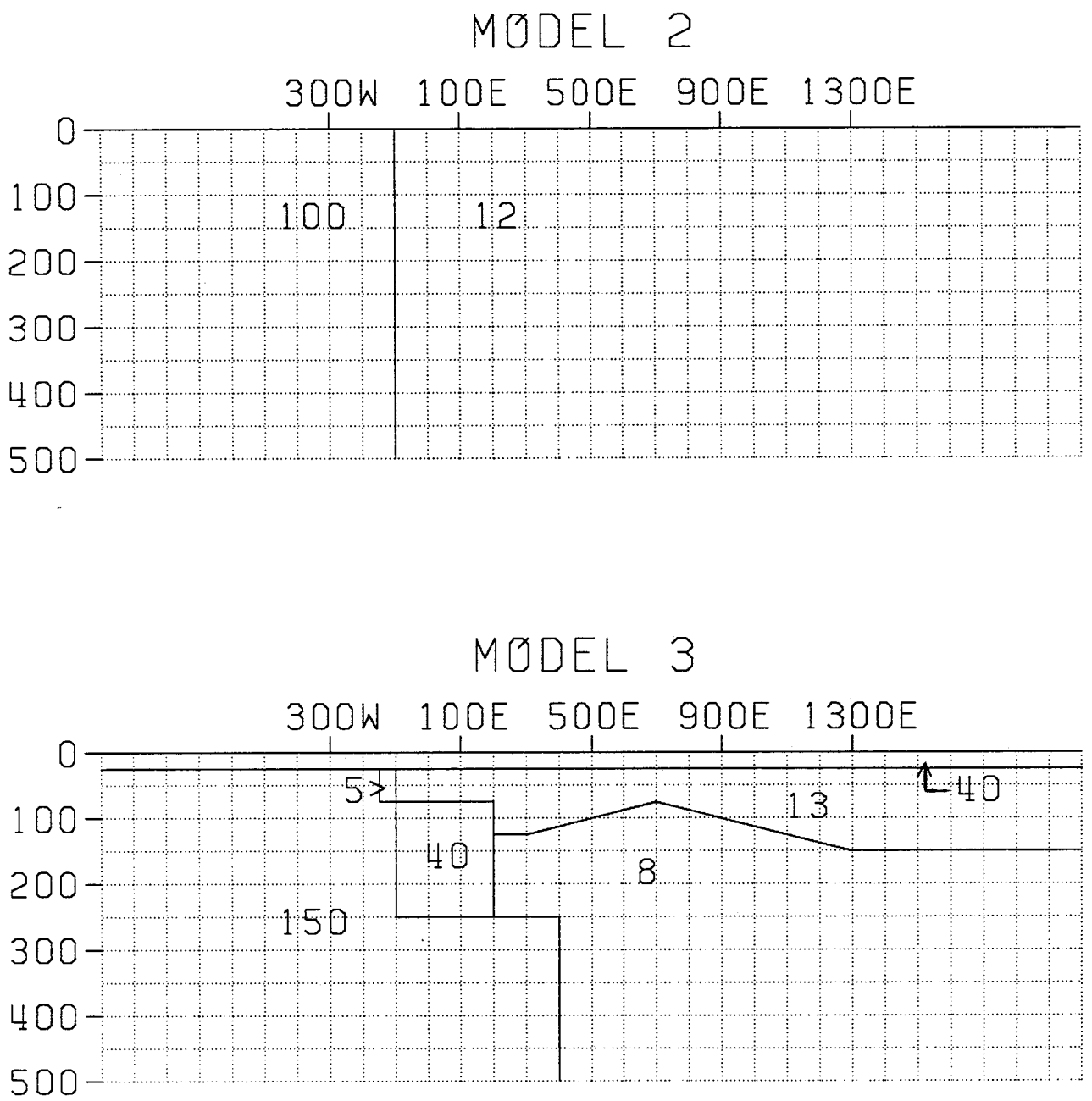

Figure 27 The starting models used for (a) Model 2, and (b) Model 3. Resistivities are in ohm-m. Horizontal scale is 1" = 500 m. Vertical scale is 1" - 250 m. Vertical exaggeration is 2:1.

Figure 28 is an image of the geoelectric section derived from the vertical contact starting model of Figure 27(a). The lower fault block is readily apparent since it was directly interpreted in the current distribution interpretation phase. However, testing of the boundaries defining this block showed that its position is not completely resolved. Equivalent fit to the data could be achieved with the block extending further east another 100 to 200 meters and/or beginning slightly deeper. The upper fault block is only weakly indicated in the resistivity image by zones reaching up to approximately 25 ohm-m. This block is, however, clearly evident in the current distribution interpretations. This shows that improvement in the image resistivity stacking process can still be made. The strong resistivity gradient apparent underneath position 100 W is due to the starting model resistivity contrast across the boundary at that position.

The structural model interpreted from Figure 28 and the knowledge gained from the current distribution interpretation phase is that presented in Figure 27(b). A brief example of assessing how well the method has performed up to this point is provided in Figure 29. Here the measurements are compared to calculations for the new starting model (the interpretation already achieved) at time 2.2 msec. It can be seen that a pretty good match exists for the data for transmitters 1300 E, 900 E and 100 E. A big amplitude discrepancy exists for transmitter 500 E which relates to the resistivity of the basin fill and significant overall differences still exists for transmitter 300 W. The overall match is already relatively good after just this one iteration. The second iteration therefore will primarily serve to simply refine the structural interpretation.

Figure 30 displays the image resistivity section derived from the refined starting model of Figure 27(b). The major features to observe in this section are that both fault blocks appear to have resistivities lower than the unfaulted Paleozoic rock further to the west. The range appears to be between approximately 40 to 100 ohm-m. In addition there is a low resistivity feature, in the range from 10 to 20 ohm-m, at the base of the upper fault block. It is unknown whether this feature is real, as no geologic data on this zone is available, or is an artifact of the imaging procedure in some undetermined way. It is geologically plausible, however, for such a zone to exist.

In principle the iterative imaging process may continue to whatever degree of data fit and model invariance is deemed appropriate. The present interpretation, however, is sufficient for purposes of illustrating the capabilities and convergence characteristics of the 2-D imaging method.

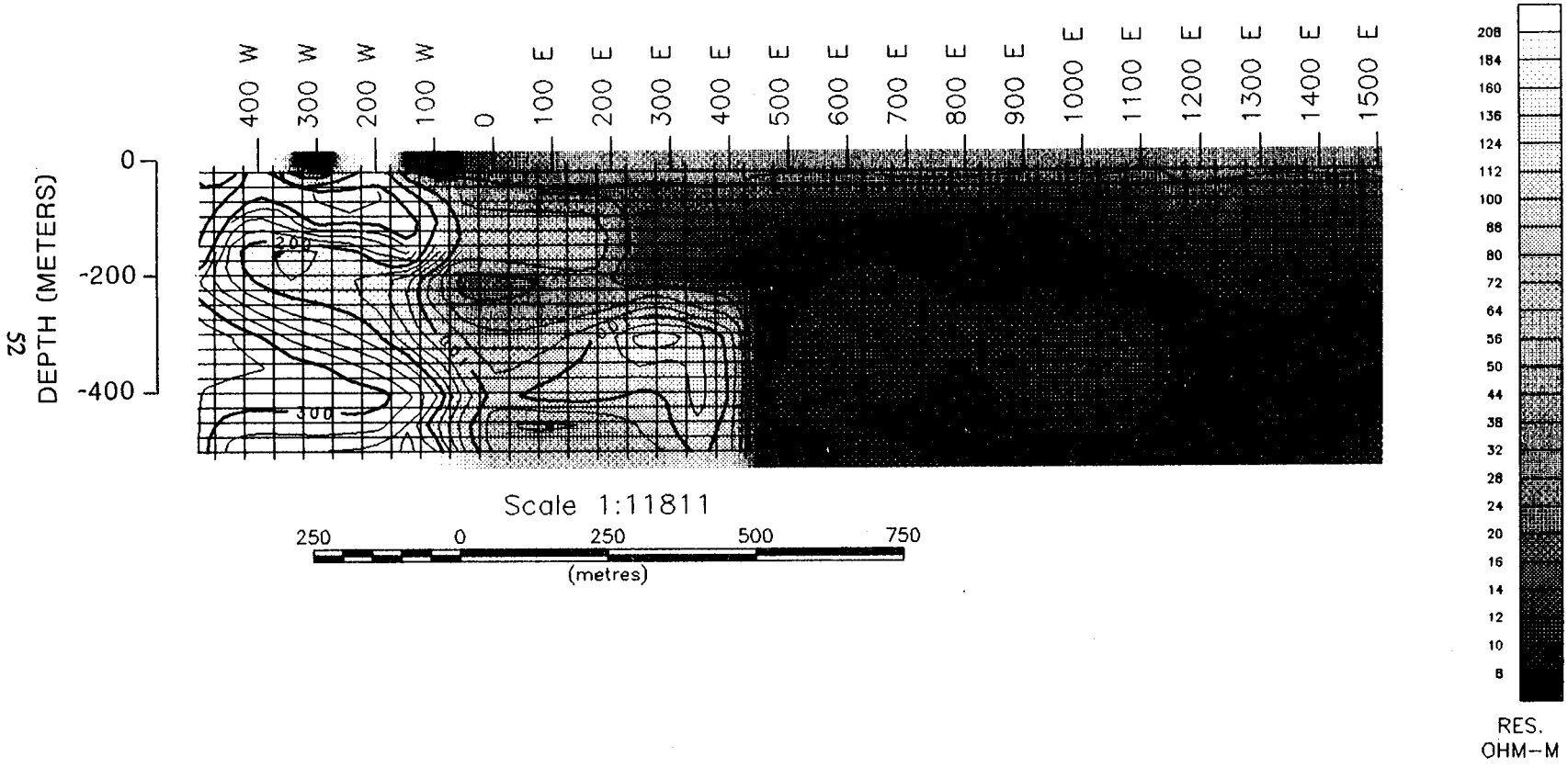

Figure 28 Imaged resistivity section for Model 2.

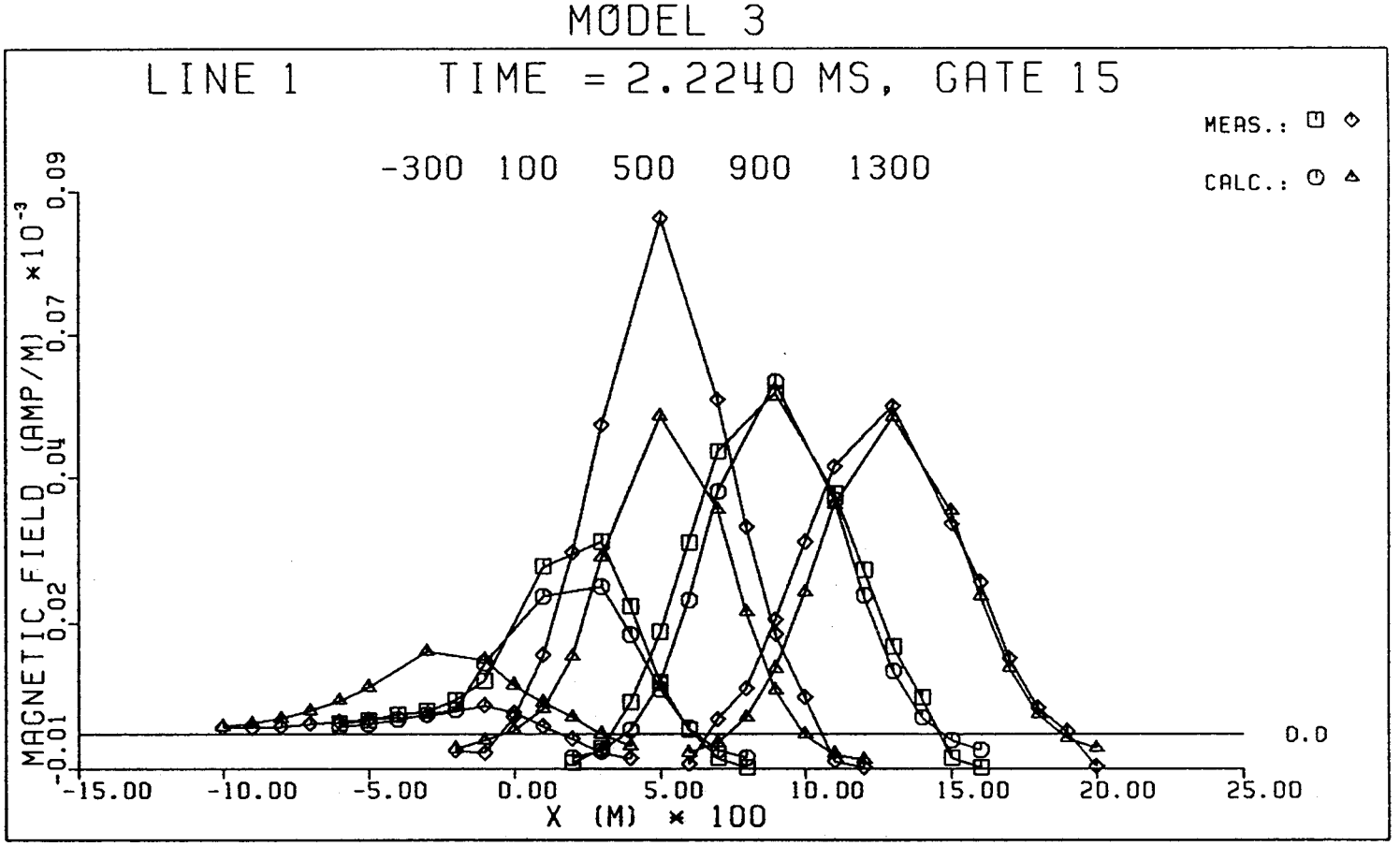

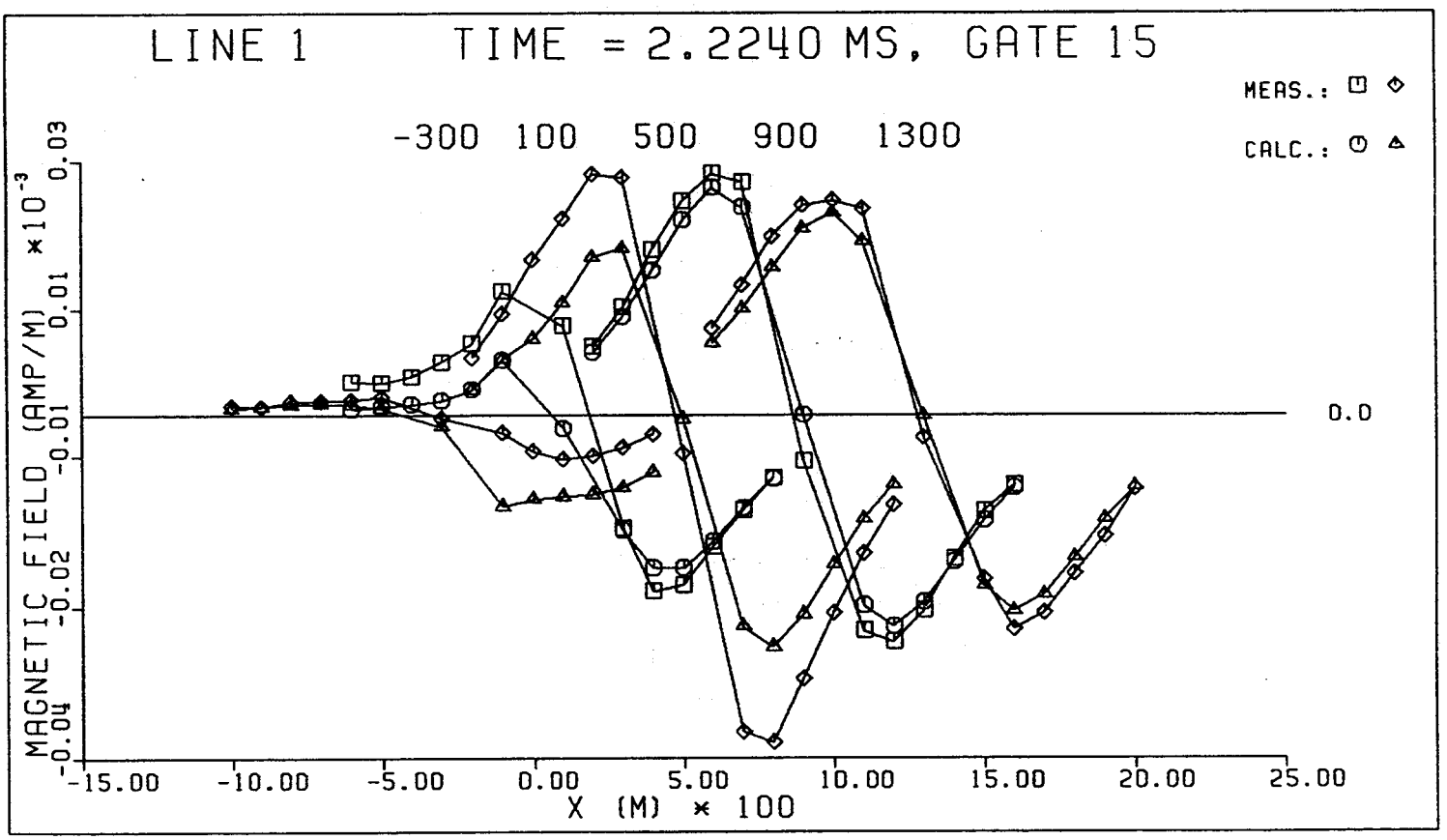

Figure 29 Sample profile time slices of the fit of calculations for the model displayed in Figure 28(b) to the measured data for (a) the z-component, and (b) the x-component.

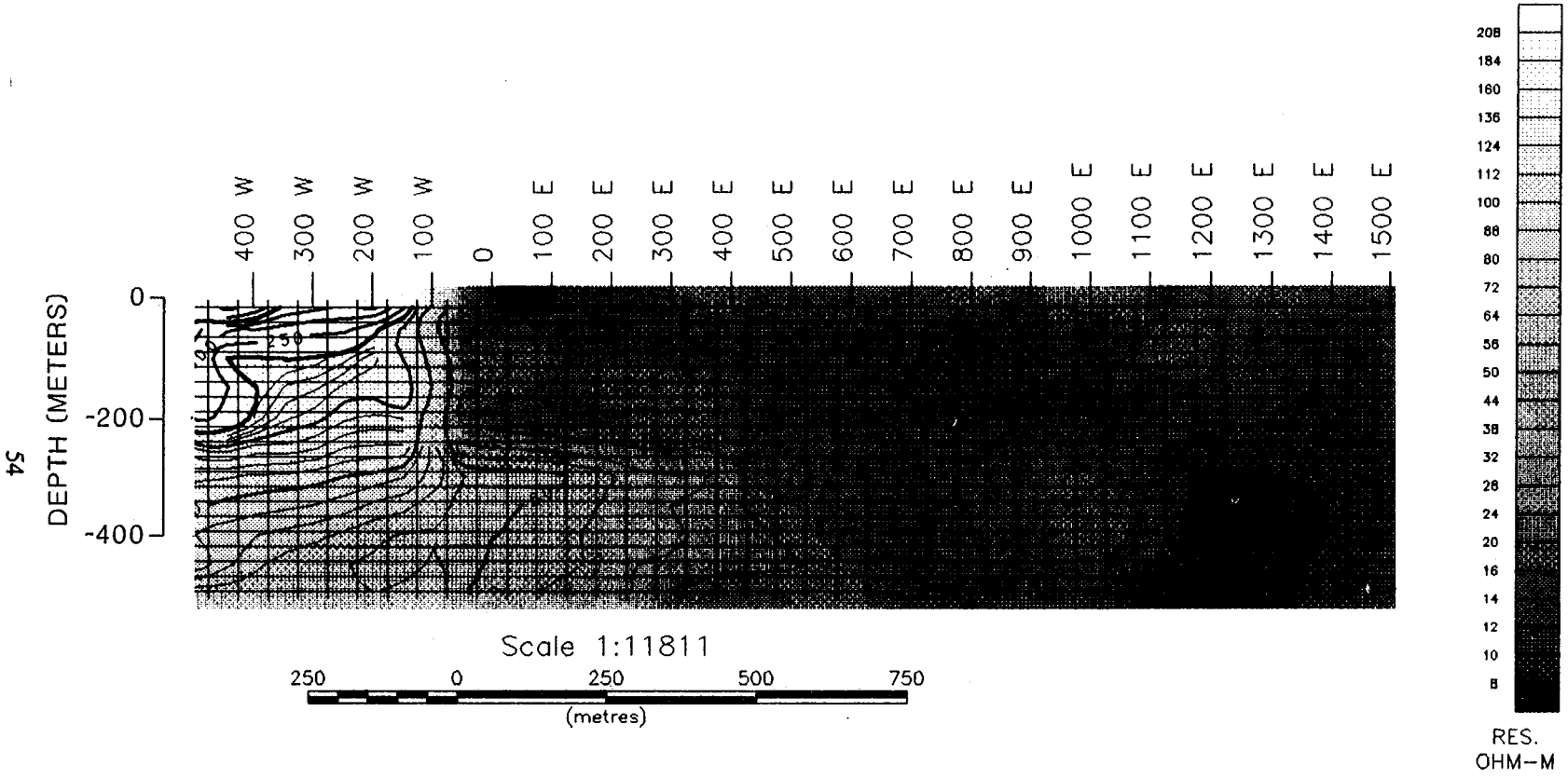

Figure 30 Imaged resistivity section for Model 3.

4.6 Conclusions

Comparing the geoelectric section derived from 2-D imaging with known geology, it can be concluded that it produces a geoelectric section at the present time better than the geoelectric section derived from 1-D imaging. It is inherently subjective to say specifically how much better it is. However, the results of the research on 2-D imaging show that:

1) It has been proven that the 2-D imaging method is basically sound, and that from the current distribution in the earth the magnetic fields can be computed and compared to measured data. Matching is performed simultaneously on both horizontal and vertical magnetic field components, and this is a major improvement on 1-D inversion and 1-D imaging interpretations. However, the method does usually require multiple imaging iterations with the quality of the image resistivity section being a function of the closeness of the starting model to the final model.

2) The 2-D imaging method is flexible in the type of structure it can accommodate. The chosen test site provides strong structural effects that are about as strong as could be conceived. However, it is necessary that general numerical modeling capability be available as a complementary technology.

3) The 2-D imaging provided information on both structure and fault block resistivity bounds that was unavailable in 1-D methods. However, exact resolution is still not obtained. Ambiguity in EM interpretation will always exist.

The improvements required to bring these types of procedures into full routine practice appear from here on out to be more technical than fundamental. The iterative process of perturbing current distribution needs to be further automated, the stacking process used to create the image resistivity section can be further refined, the influence of initial model on final results needs to be better understood, and graphical presentations can be enhanced. One especially attractive feature of this imaging approach is that it yields a thorough physical understanding of current flow in the ground. This in turn may be useful in survey design exercises for optimum layout of transmitter and receiver loops.

5.0 CONCLUSIONS

The R&D program reported above had as its objectives improvement in the interpretation of TEM data over 2-D geoelectric structures. The work proceeded along three linked paths, (i) acquisition of high density data sets, (ii) development of programs for forward modeling of 3-D transient fields over 2-D geoelectric structures, and (iii) 2-D imaging of high density TEM data over 2-D structures.

A test site was selected in the Basin and Range province of Nevada, and data were acquired over a profile perpendicular to the main Basin and Range fault. At this site ground truth was available from detailed geologic mapping, several drill holes, and other geophysical surveys. The geoelectric structure is similar to those of the Trap Springs and Grant Canyon oil fields in Railroad Valley, Nevada. Over this test site a high density data set was acquired with receiver positions electromagnetically illuminated from several transmitter positions. Also, three components of the EM fields were measured at each receiver location.

The data were acquired with commercially available TEM equipment. This equipment is designed for the typical station density acquisition common in the industry. Should the practice of high density data acquisition and its advantages of higher resolution become accepted, then multi-channel, 3-component acquisition receivers should be developed.

In addition to processing the data with a 2-D imaging method developed under this program, they were also analyzed and interpreted by conventional 1-D inversion and 1-D imaging procedures, so that the limitations of the 1-D analysis can be understood.

Comparing the results of the geoelectric section derived from 1-D interpretations with the known geologic section, it can concluded that:

1) The 1-D imaging and 1-D inversion of the EM fields due to the time derivative of the vertical magnetic field employing non-grounded transmitter loops, results in a geoelectric section that correlates reasonably well with known geology. Particularly, the location and depth of the fault can be approximately located from 1-D analysis.

2) The main distortion resulting from 1-D analysis is in the absolute values of resistivity. Often phantom resistivity stratifications arise that do not correlate with known geology.

The direction chosen for modeling 3-D transient EM fields over a 2-D earth was that of frequency domain finite element modeling with Fourier transformation to the time domain. Accuracy of the results of the program were verified by comparing numerical results to analytical solutions for a homogeneous earth. Further confidence in the results was gained from their use in the 2-D imaging algorithms, which produced a geoelectric section consistent with known geology and 1-D inversion and imaging. The computation of 3-D EM fields over a 2-D structure remains a formidable task, and the hardware required is still more than commonly available on PC's. Computations were carried out on a MicroWay Number Smasher 860 board running at 33 MHz with 8 Mb of ram memory. This board was fitted into a ALR Power VEISA with a 33 MHz 386 processor, 64Kb Cache, 5 Mb of RAM memory and a 100 Mb hard disk. Each model run took 12 hours (at approximately 9 MFLOPS) for a mesh size of 36 (vertical) by 169 (horizontal) nodes.

The computer resource required for finite element modeling of EM fields precludes for some time its effective use in inversion routines. However, forward modeling is a necessary capability in analyzing and planning TEM surveys. The results of numerical computations are needed for validating geoelectric sections derived from 2-D imaging, and for providing synthetic data sets for (i) determining the range of applications and limitations of 1-D interpretations, and (ii) design of survey parameters for 2-D imaging interpretation.

The TEM subsurface 2-D imaging method developed under this program derives the geoelectric section following the intermediate step of imaging the electrical current distribution in the ground. It utilizes a complete representation of distributed current flow on a subsurface grid, so that it can accommodate complicated geologic structures. The imaging process begins by computing the current distribution, as a function of time, for an initial model and subsequently perturbs the current flow by an iterative process until a match is obtained between measured and computed magnetic fields. The magnetic fields are calculated from the current distributions using Biot-Savart's Law. Once all current distributions are interpreted, a resistivity image is created from a selective summation of the current in each pixel relative to the current in that pixel for the initial model.

A synthetic data set derived from forward modeling was used to test the imaging algorithms, and the method was subsequently employed in the analysis of the test data set to produce a geoelectric section. The 2-D image is superior to the 1-D image in that it yields sharper resistivity contrasts and does not produce phantom zones of the type seen in the 1-D imaging. The significant results of the 2-D imaging at this time are:

1) It has been proven that the 2-D imaging method is basically sound, and that from the current distribution in the earth. The magnetic fields can be computed and compared to measured data. Matching is performed simultaneously on both horizontal and vertical magnetic field components.

2) The 2-D imaging method is flexible in the type of structures it can accommodate.

3) The geoelectric section produced from the 2-D imaging process compares well with known geology and is an improvement on the geoelectric sections derived from 1-D inversions and 1-D imaging.

The grounded line data acquired in this project were not interpreted with the 2-D imaging method, because this was beyond the scope of this project. It will be interesting to evaluate what additional information these data bring to the imaging scheme when interpretation of these data becomes possible. Effective application of the imaging method requires a high density TEM data set with electromagnetic illumination of receiver locations from multiple transmitters. Both transmitter and receiver locations are needed on regularly spaced profiles, and 3-component measurements need to be recorded. The improvements required to bring 2-D imaging into regular practice appear to be routine in nature, such as fully automating the iterative process of perturbing current distributions.

6.0 REFERENCES

Anderson, W.L., 1979. Programs TRANS_HCLOOP and TRANS_HZWIRE: calculation of the transient horizontal coplanar loop soundings and transient wire-loop soundings: U.S.G.S. Open File Report 79-590, 46 p.

Bernstein, G.L., M.M. Mandelhaum, M.B. Rappaport, M.V. Schornikova, 1977. Methods characteristic of direct prospecting for oil and gas deposits on the southern slope of Nepsky arch, Moscow, A-USR IYGG, Department of Scientific Technical Information.

Blackhawk Geosciences, Inc., 1991, Topical Report: Acquisition and One-Dimensional Interpretation of Transient Electromagnetic (TEM) Data; prepared for U.S. Department of Energy, DOE Contract No. DE-AC22-90BC14476.

Duey, H.D., 1979. Trap Spring oil field, Nye County, Nevada, in Newman, G.W. and Goode, H.D., eds. Basin and Range Symposium: Rocky Mountain Association of Geologists and Utah Geological Association, p. 469-476.

Eaton, P. A. and Hohmann, G. W., 1989, A rapid inversion technique for transient electromagnetic soundings: Phys. Earth Plan. Int., 53, 384-404.

Hoekstra, P. and M.W. Blohm, 1990. Case histories of time-domain electromagnetic soundings in environmental geophysics, in Geotechnical and Environmental Geophysics, Vol. II, 1-15, S. H. Ward, ed.

Hoekstra, P., J. Hild and M.W. Blohm, 1989. Geophysical surveys for precious metal exploration in the Basin and Range, Nevada, in Proc. Gold Forum on Technology and Practices, World Gold '89, Soc. Mining, Metallurgy and Exploration, CO.

Hohmann, G. W., 1992, personal communication, at annual sponsors meeting for Consortium for Electromagnetic Modeling and Inversion, February 28.

Inman, J.R., 1975. Resistivity inversion with ridge regression: Geophysics, V. 40, 798-817.

Interpex Limited, 1990. Topical Report, Direction of Research for Development of 2.5-D Forward Modeling and Imaging of TEM Data: U.S. DOE, Contract No: DE-AC22-90BC14476.

James Consulting Services, Inc., 1990, Topical Report: TEM Imaging via Interpretation of Current Distributions: prepared for U.S. Department of Energy, DOE Contract No. DE-AC22-90BC14476.

Keller, G.V., J.I. Pritchard, J.J. Jackson, and N. Harthill, 1984. Megasource time domain electromagnetic soundings methods. Geophysics, V 49, 993-1009.

Lacoste, L. J. B., 1982, Deconvolution by successive approximations: Geophysics, 47, 1724-1730.

Lee, K. H. and Morrison, H. F., 1985, A numerical solution for the electromagnetic scattering by a two-dimensional inhomogeneity: Geophysics, v 50, pp 466-472.

Macnae, J. and Lamontagne, Y., 1987, Imaging quasi-layered conductive structures by simple processing of transient electromagnetic data: Geophysics, 52, 545-554.

Nekut, A. G., 1987, Direct inversion of time-domain electromagnetic data: Geophysics, 52, 1431-1435.

Newman, G. A., Hohmann, G. W., and Anderson, W. L., 1986, Transient electromagnetic response of a three-dimensional body in a layered earth: Geophysics, 51, 1608-1627.

Newman, G. A. and Hohmann, G. W., 1987, Interpretation of TEM soundings over 3-D structures with the central-loop configuration: Geophys. J. Roy. Astr. Soc., 89, 889-914.

Rodi, W. L., 1976, A technique for improving the accuracy of finite element solutions for magnetotelluric data: Geophys. J. R. astr. Soc., v 44, pp 483-506.

Stoyer, C. H. and Greenfield, R. J., 1976, Numerical solutions of the response of a two-dimensional earth to an oscillating magnetic dipole source: Geophysics, v 41, pp 519-530.

Swift, C. M., 1971, Theoretical magnetotelluric and turam response from two-dimensional inhomogeneities: Geophysics, v 36, pp 38-52.

Valla, Pierre, 1991, Applications de la modélisation numérique aux méthodes d'électromagnétisme fréquentiel en prospection géophysique: Document du BRGM n° 206, Éditions du BRGM, Orléans, FRANCE, 471 p.

Wannamaker, P. E. and J. A. Stodt, 1987, A stable finite element solution for two-dimensional magnetotelluric modeling: Geophys. J. R. astr. Soc., v 88, pp 277-296.

Wilt, M.J., 1991. Interpretation of time domain electromagnetic soundings near geologic contacts, Ph.D. Thesis, Lawrence Berkeley Laboratory, Unv. of California at Berkeley.

*U.S.GPO:1992-661-026/60045